Heliyon 10 (2024) e27417

Contents lists available at ScienceDirect

Heliyon

journal homepage: www.cell.com/heliyon

Research article

Designing a conjugate vaccine targeting *Klebsiella pneumoniae* ST258 and ST11

Min Li [a], Mingkai Yu [b], Yigang Yuan [a], Danyang Li [a], Daijiao Ye [a], Min Zhao [a], Zihan Lin [a], Liuzhi Shi [c,*]

[a] *Medical Research Center, The First Affiliated Hospital of Wenzhou Medical University, 1 Xuefubei Street, Ouhai District, Wenzhou, Zhejiang Province, China*
[b] *School of Life Science and Technology, Southeast University, Xinjiekou Street, Xuanwu District, Nanjing, Jiangsu Province, China*
[c] *Department of Clinical Laboratory, Key Laboratory of Clinical Laboratory Diagnosis and Translational Research of Zhejiang Province, The First Affiliated Hospital of Wenzhou Medical University, Wenzhou, Zhejiang Province, China*

ARTICLE INFO

Keywords:
Klebsiella pneumoniae
Drug resistance
Multi-epitope vaccine
Immunoinformatics

ABSTRACT

Klebsiella pneumoniae (*K. pneumoniae*) is a common bacterium that can cause iatrogenic infection. Recently, the rise of antibiotic resistance among *K. pneumoniae* strains is one key factor associated with antibiotic treatment failure. Hencefore, there is an urgent need for effective *K. pneumoniae* vaccines. This study aimed to design a multi-epitope vaccine (MEV) candidate against *K. pneumonia* by utilizing an immunoinformatics method. In this study, we obtained 15 cytotoxic T lymphocyte epitopes, 10 helper T lymphocyte epitopes, 6 linear B-cell epitopes, and 2 conformational B-cell epitopes for further research. Then, we designed a multi-epitope vaccine composed of a total of 743 amino acids, containing the epitopes linked by GPGPG flexible links and an EAAAK linker to the Cholera Toxin Subunit B coadjuvant.

The observed properties of the MEV, including non-allergenicity, high antigenicity, and hydrophilicity, are noteworthy. The improvements in the tertiary structure through structural refinement and disulfide bonding, coupled with promising molecular interactions revealed by molecular dynamics simulations with TLR4, position the MEV as a strong candidate for further investigation against *K. pneumoniae*.

1. Introduction

Klebsiella, a gram-negative rod-shaped bacterium, is an opportunistic pathogen, which causes various diseases in humans and animals. The Klebsiella genus comprises eleven identified species, namely *Klebsiella pneumoniae* (*K. pneumoniae*), *Klebsiella ornithinolytica, Klebsiella terrigena, Klebsiella africanensis, Klebsiella oxytoca, Klebsiella granulomatis, Klebsiella planticola, Klebsiella variicola, Klebsiella quasipneumoniae, Klebsiella aerogenes*, and *Klebsiellagrimontii* [1]. Klebsiellar pneumonia, an important type of pneumonia typically in the form of bronchopneumonia and also bronchitis, is caused by *K. pneumoniae* [2]. Notably, Kp is further classified into classical (cKp) and hypervirulent (hvKp) strains based on their phenotype and pathogenicity [3,4]. Generally, cKp primarily causes infections in immunocompromised individuals, such as patients receiving chemotherapy, the elderly population, and newborns. In contrast, hvKp is responsible for a broader spectrum of infections and can affect individuals of any age who are in good health [5].

* Corresponding author.
E-mail address: liuzhishi@wmu.edu.cn (L. Shi).

https://doi.org/10.1016/j.heliyon.2024.e27417
Received 22 September 2023; Received in revised form 28 February 2024; Accepted 28 February 2024
Available online 8 March 2024

Abbreviations

K. pneumoniae	Klebsiella pneumoniae
Kp	K. pneumonia
KPC-Kp	KPC-producing K. pneumoniae
MLST or ST	Multilocus sequence type
CG258	Clonal group 258
OMVs	Outer membrane vesicles
LPS	Lipopolysaccharide
Omps	Outer membrane proteins
OmpA	Outer membrane protein A
OmpC	Outer membrane protein C
E. coli	Escherichia coli
RBP	Receptor binding protein
Ompk37	Outer membrane protein k37
MD	Molecular dynamics
BLASTp	Protein Basic Local Alignment Search Tool
CARD	Comprehensive Antibiotic Resistance Database
KEGG	Kyoto Encyclopedia of Genes and Genomes
CTB	Cholera toxin B subunit
LTA1	Heat-labile toxin
SOPMA	Self-optimized prediction method
PCA	Principal component analysis
JCAT	JAVA Codon adaptation tool
MCS	Multiple cloning site
XDR-KP	Extensively drug-resistant Klebsiella pneumoniae
CZA	Ceftazidime-avibactam
HLA	Human leukocyte antigen
GRAVY	A grand average of hydropathicity
TLR4	Toll-like receptor 4

Additionally, many cases of KPC-producing Enterobacteriaceae, in particular *K. pneumoniae*, have been reported in various countries. In 2019, the KPC-producing *K. pneumoniae* (KPC-Kp) was reported to have caused millions of deaths. However, there are no existing vaccines available in the market to tackle KPC-Kp. Given the severity of the disease, the development of a safe and effective vaccine to fight against the KPC-Kp is urgently needed.

The global dissemination of KPC-Kp is linked to a predominant multilocus sequence type (MLST or ST). The vast majority of KPC-Kp isolates worldwide belong to the clonal group 258 (CG258), and the two major sequence types are ST258 (ST allele profile, 3-3-1-1-1-1-79) and its single-locus variation ST11 (3-3-1-1-1-1-4) [6]. Among these, ST258 is predominantly found in Europe and the United States, while ST11 emerges as the prevailing clone in Asian countries, particularly China [7]. Therefore, we have selected ST258 and ST11 as our primary research targets due to their high prevalence. Currently, the primary immunization strategies against *K. pneumoniae* encompass outer membrane vesicles (OMVs), lipopolysaccharide (LPS), whole cell vaccines (live attenuated bacteria, inactivated whole cells, and cell extracts), polysaccharide, ribosome, bioconjugate vaccine, and multi-epitope vaccines (MEVs) [8,9]. According to the report, the constructed MEVs exhibit a high potential for stimulating both B and T-cells immune responses against pneumonia infection [10]. In addition, MEVs are designed to enhance efficiency and cost-effectiveness by obviating the necessity for microbial culture, selecting epitopes that encompass a broad spectrum of alleles, and circumventing the biohazardous nature and potential toxicity associated with conventional inactivated or attenuated vaccines [11]. Furthermore, investigations have been conducted on MEVs targeting various pathogens including *Echinococcus granulosus*, *Staphylococcus aureus*, SARS-CoV-2, and *Salmonella* [12–15].

Finding highly conserved and stable antigens from *K. pneumoniae* strains has emerged as a focal point of research. *K. pneumonia* primarily relies on the outer membrane proteins (Omps), LPS (O antigen), and capsular polysaccharide (K antigen) (CPS) to evade the host immune response [16]. Omps act as water-filled channels that allow hydrophilic molecules to cross the membrane. These are associated with antibiotic resistance mechanisms and contribute to the virulence of the organism. Omps derived from *K. pneumoniae* have been recognized as safe subunit vaccines, exhibiting their potential by eliciting host-specific antibodies and demonstrating efficacy in animal models even without additional adjuvants, thereby rendering them suitable candidates for vaccine development. Outer membrane protein A (OmpA), also known as P40, represents a promising candidate for vaccine design due to its ubiquity in all strains [17]. Moreover, it plays a crucial role in host cell recognition, internalization, and pathogenicity, thereby influencing the innate immune response [18]. Additionally, outer membrane protein C (OmpC), alternatively known as Ompk36, exhibits 87% sequence identity with *Escherichia coli* (*E. coli*) and serves as an indispensable receptor-binding protein (RBP) in *K. pneumonia* [19]. Targeting the outer membrane protein X (OmpX), previous studies have demonstrated that specific adjuvant binding can induce a robust population

of antigen-specific $CD4^+$ tissue-resident memory (TRM) cells, making it an excellent option for vaccine design [20]. In addition, as one of the most common immunogenic proteins, outer membrane protein W (OmpW) is also a favorable selection for vaccine design [21]. Furthermore, outer membrane protein k37 (Ompk37) which acts as a porin in the outer membrane of *K. pneumoniae* and is associated with drug resistance in physiological settings, has been selected as another target in our subsequent investigations [22]. Therefore, we choose these candidate proteins as the focus of the next step.

Adjuvants play a key role in vaccines by augmenting the development of protective immune responses in both healthy individuals and those with compromised immune systems. Furthermore, strong systemic and mucosal immunity can be induced by appropriate mucosal adjuvant. Most importantly, vaccines linked to adjuvants can trigger a strong immune response in vivo [23]. The Linkers can be categorized into flexible linkers, rigid linkers, and cleavable linkers. Opting for rigid linkers is more advantageous as it helps maintain the stability or biological activity of fusion proteins, such as linker-AAY, linker-GPGPG, linker-KK, and linker-EAAAK [24]. Therefore, during the design of our vaccine, we incorporated specific linkers to complement the dominant cell epitopes and linked them to adjuvants that enhance mucosal immune responses. Finally, the vaccine complex was evaluated through methods such as molecular docking, molecular dynamics (MD) simulation, and immune simulation. A flowchart of the vaccine design is shown in Fig. 1. In conclusion, it is anticipated that this MEV can serve as a theoretical foundation for further research on a vaccine against *K. pneumoniae*.

2. Methodology

2.1. Selection of target antigens

Firstly, sequence numbers of candidate proteins and FASTA sequences were obtained from the NCBI Protein Database. Additionally, we conducted a comprehensive search for recent research on *K. pneumoniae* and specifically selected *K. pneumoniae* ST258 and ST11-associated proteins for further analysis. Thirdly, we employed ProtParam (http://web.expasy.org/ProtParam/) and VaxiJen (http://www.ddg-pharmfac.net/vaxijen/VaxiJen/VaxiJen.html) to assess the physicochemical properties of the target proteins, focusing on stability, hydrophilicity, and high antigenicity in order to identify suitable candidates for subsequent analysis [25,26]. Furthermore, the protein sequences of *K. pneumoniae* ST258 and ST11 were compared, and highly stable sequences of these two lineages were selected as potential candidate proteins. Subsequently, candidate proteins were subjected to blast in the protein Basic Local Alignment Search Tool (BLASTp) of NCBI to rule out human-derived proteins [27]. In addition, the Comprehensive Antibiotic Resistance Database (CARD) (https://card.mcmaster.ca/analyze/blast) was used to identify proteins of different strains exhibiting significant homology in order to investigate their potential for inducing cross-immune reactions [28]. Moreover, three different servers were used for protein functional analysis, namely UniProt (https://www.uniprot.org/), Kyoto Encyclopedia of Genes and Genomes (KEGG), and InterPro (https://www.ebi.ac.uk/interpro/). These analyses predicted the classification of protein families as well as their biological processes and molecular functions. Finally, we employed Jalview to compare the homology among these five candidate proteins [29].

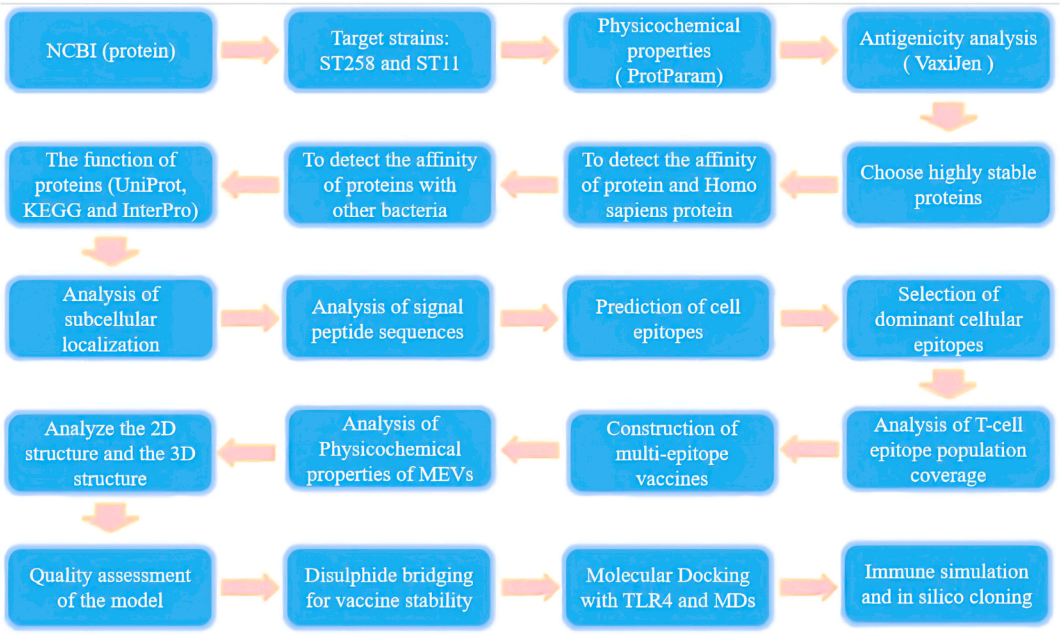

Fig. 1. Illustration of chimeric multi-epitope vaccine (MEV) design.

2.2. Prediction of target protein subcellular localization and signaling peptides

DeepTMHMM v1.0.11 (https://dtu.biolib.com/DeepTMHMM) is the most complete and effective method to predict the topological structure of α-helix and β-barrel transmembrane proteins. The model encodes the primary amino acid sequence by a pre-trained language model, and decodes the topology by a state space model, generating topology and type prediction with unprecedented accuracy. Therefore, DeepTMHMM was used to predict the subcellular localization of proteins. Proteins located on the surface of the cell membrane are good candidates for designing vaccines [30]. SignalP-6.0 (https://services.healthtech.dtu.dk/service.php?SignalP) was used to further pinpoint signal peptide sequences. SignalP-6.0 (https://services.healthtech.dtu.dk/service.php?SignalP) can be used to identify five different types of signal peptides. Sec/SPI was the standard secretory signal peptides, transported by the Sec translocon and cleaved by Signal Peptidase I. Sec/SPII was the lipoprotein signal peptides, transported by the Sec translocon and cleaved by Signal Peptidase II. Tat/SPI was the Tat signal peptides, transported by the Tat translocon and cleaved by Signal Peptidase I. Tat/SPII was the Tat lipoprotein signal peptides, transported by the Tat translocon and cleaved by Signal Peptidase II. Sec/SPIII was the Pilin and pilin-like signal peptides, transported by the Sec translocon and cleaved by Signal Peptidase III [31].

2.3. Prediction of CTL cell epitopes

First, we used the online tool of the IEDB analysis resource (http://tools.iedb.org/mhci/) to predict CTL epitopes. Furthermore, we selected 27 highly expressed alleles for analysis. According to the study, there are 27 alleles with high frequency in the world, covering 97% of the global population [32]. Therefore, we selected epitopes that appeared more than or equal to 10 times in these genes as dominant CTL epitopes.

2.4. Prediction of HTL cell epitopes

Firstly, HTL epitopes were determined using the MHC-class II binding allele prediction tool IEDB (http://tools.IEDB.org/mhcii/). Furthermore, 27 alleles with a high prevalence of HLA-II in the population were selected for comprehensive analysis. Then, the output length was 15 amino acids. Finally, sequences with a percentile rank of less than or equal to 5 and present in greater than or equal to 10 alleles were selected as dominant HTL epitopes.

2.5. Prediction of B cell epitopes

Firstly, we used ABCpred (https://webs.iiitd.edu.in/raghava/abcpred/ABC_submission.html) to predict linear B cell epitopes. ABCpred mainly uses artificial neural network algorithms in the prediction process [33]. Subsequently, amino acid sequence was utilized as input with a threshold set at 0.51 and a fixed amino acid length of 16. Next, we defined dominant linear B cell epitopes as those with a score greater than 1 and an antigenicity greater than 1.4. Prediction of conformational B-cell epitope requires the tertiary structure of target protein. But there is currently no relevant tertiary structure in the UniProt database. Alphafold incorporates novel machine-learning techniques that integrate physical and biological knowledge of protein structure to develop deep learning algorithms using multiple sequence alignments, making predictions more accurate [34]. Therefore, Alphafold was utilized for the prediction of the structural conformation of five proteins. The SWISS-MODEL structure evaluation service (https://swissmodel. expasy.org/assess) was used to evaluate the accuracy of the predicted proteins. Additionally, ElliPro (http://tools.iedb.org/ellipro/) was used to predict conformational B cell epitopes [35]. In terms of parameter settings, the minimum score is set to 0.5 and the maximum distance is set to 6.

2.6. Selection of dominant cell epitopes and adjuvant

Firstly, we used VaxiJen to analyze the antigenicity of individual epitopes and screen out epitopes with a threshold above 0.4. In addition, epitopes with high antigenicity were analyzed by AllergenFP (http://www.ddg-pharmfac.net/AllergenFP/), and non-allergenic epitopes were screened out [36]. Therefore, the epitopes with antigenicity greater than 0.4 and non-allergenic were selected to construct MEVs. In terms of adjuvant selection, two distinct adjuvants were separately chosen for analysis. The cholera toxin B subunit (CTB) and *Escherichia coli* heat-labile toxin (LTA1) have been used as potent mucosal adjuvants, making them optimal choices for vaccine design [37]. Then, the structure of the two proteins was analyzed using DeepTMHMM, and the sequences located in the extracellular membrane were selected. Finally, in order to remove the signal peptide sequence in adjuvants, we used SignalP-6.0 to delete the signal peptide.

2.7. Analysis of population coverage of the T epitopes

Due to the high variability of peptide-binding regions in MHC molecules, they exhibit a broad range of binding specificity [38]. To address this issue, it is necessary to determine the proportion of individuals expected to respond to the vaccine based on HLA genotypic frequencies. Estimating population coverage through IEDB (http://tools.iedb.org/population/) simplifies complexity and reduces variability in achieved or predicted coverage across different ethnic groups [39].

2.8. Construction of multi-epitope vaccines

The epitopes were chosen based on their wide allele coverage, high antigenicity, non-sensitization, and non-toxicity, making them the dominant epitopes. To connect CTL cell epitopes, a rigid AAY linker was selected; for HTL cell epitopes, a GPGPG linker was chosen; and B cell epitopes were connected using the KK linker. Additionally, an EAAAK linker was attached to the N-terminal of the epitope vaccine. Finally, two adjuvants (CTB and LTA1) were selected to construct MEVs. The candidate vaccine was exhibited high antigenicity and favorable physicochemical properties.

2.8.1. Analysis of the physicochemical properties of vaccines

Firstly, VaxiJen was employed to assess the antigenicity of the MEVs. Secondly, AllergenFP was utilized to evaluate the sensitization of the MEVs. Then, ProtParam was applied to analyze the physicochemical properties of the vaccine. Fourthly, SOLpro (http://scratch.proteomics.ics.uci.edu/) was used to analyze the solubility of the MEVs [40]. Finally, the hydrophobicity analysis was conducted using the ProtScale server (https://web.expasy.org/protscale/). Ultimately, a comprehensive evaluation led to selecting a candidate vaccine with high antigenicity, non-sensitization, with good physicochemical properties, high solubility, and strong hydrophilicity.

2.8.2. Prediction, refinement, and validation of 3D vaccine construct

First of all, the improved self-optimized prediction method (SOPMA) (http://npsa-pbil.ibcp.fr/cgi-bin/npsa_automat.pl?page=/npsa/npsa_sopma.html) has demonstrated a remarkably high success rate in accurately predicting secondary structures [41]. Therefore, we employed SOPMA to predict the secondary structure of MEV1. During this prediction process, our focus primarily lied on analyzing the proportion of random coil and β-turn within the protein. Furthermore, we utilized Alphafold, renowned for its exceptional prediction accuracy, to forecast the tertiary structure of MEV1. By employing these highly accurate forecasting methods, we enhanced precision in subsequent analyses. Subsequently, we leveraged the GalaxyRefine web server (https://galaxy.seoklab.org/) to optimize protein structure that based on sequence information through template-based modeling and refined loop or terminal regions via ab initio modeling techniques. This approach significantly improved the accuracy of protein models [42]. Therefore, the GalaxyRefine web server was used to refine the predicted model of the MEV1. Subsequently, a comprehensive analysis of the model's quality was conducted utilizing the ProSA-web prediction (https://prosa.services.came.sbg.ac.at/prosa.php), ERRAT server (https:/servicesn.mbi.ucla.edu/ERRAT/) and SWISS-MODEL structure assessment service prediction [43].

2.8.3. Disulphide bridging for vaccine stability

Disulphide by Design v2.12 (https://cptweb.cpt.wayne.edu/DbD2/) is an innovative way of creating vaccines and building model structures. It was specifically designed to facilitate disulfide engineering in vaccine design, aiming to enhance the stability of simulated protein structures [44]. To stabilize molecular interactions, disulfide bonds provide concise geometric confirmation. Notably, the selection of disulfide bond requires an energy fraction below 2.2 kcal/mol and an X^3 value ranging from $-87°$to $+97°$ [45].

2.8.4. Molecular docking with TLR4

The 3D structure of TLR4 was acquired from the PDB database (https://www.rcsb.org/). The HDOCK server was selected for simulated molecular docking with TLR4 as the receptor and MEV1 as the ligand. To assess model refinement and investigate the potential effects of disulfide on the interaction between the model and immune molecules, three distinct stages of MEV1 were individually docked to TLR4. Finally, PyMol and Ligplus were employed to visualize changes in both two-dimensional and three-dimensional atomic interactions [46]. In particular, PyMol facilitated visualization of docking conformations while Ligplus enabled analysis of receptor-ligand interaction forces.

2.8.5. Molecular dynamics simulation

To evaluate the deformability of the complex, B-factors, variance, and eigenvalues, MD simulations were performed on the iMODS platform (http://iMODS.chaconlab.org) [47]. Gromacs 2021.3 was selected for Molecular dynamics simulation to further evaluate the dynamic changes of the complex [48]. The optimal docking system was solvated in a rectangular box of TIP3P waters extending from the protein boundary to a minimum cutoff of 15 Å [49]. Subsequently, Na + or Cl-ions were introduced onto the protein surface to neutralize the overall charge of the system. Afterwards, the Amber ff14SB force field was used in all MD simulations [50]. With appropriate configuration, the initial structure is effectively minimized by utilizing the steepest descent and conjugate gradient method. Subsequently, the system was lightly annealed from 10 K to 300 K in the canonical ensemble for 0.2 ns, using a weak constraint of 15 kcal/mol/Å for the protein master atom. Within the isothermal-isobaric ensemble, density balance was achieved over a period of 1000 ps using Langevin-thermostat and Berendsen barostat techniques with collision frequency set at 0.002 ns and pressure relaxation time at 0.001 ns [51,52]. Following proper minimization and equilibrium establishment, 100,000 ps of efficient MD runs were performed on each system. Finally, leveraging the MMPBSA.py module of Amber Tools 20 along with the molecular mechanics-generalized-born surface area (MMGBSA) approach facilitated the calculation of combined freedom within the complex [53]. The computer simulations may not accurately depict molecular behavior due to inherent limitations in the computer model. It's imperative to exercise utmost caution when initiating the simulation process in order to obtain reliable results. Finally, we employed AMBER20, a powerful tool, for a duration of 200 ns to enhance the robustness of our simulations.

2.8.6. Principal component analysis

As a commonly used statistical technique, Principal component analysis (PCA) was used to simplify the complexity of kinetic data and extract the collective and associated motions of biomolecular atoms [54]. The position of the Cα atom in the simulation system was obtained by using the Gromacs 2021.3 software package. PC1 and PC2 were represented the first principal component and the second principal component, respectively.

2.8.7. Immune simulation

C-ImmSim (https://kraken.iac.rm.cnr.it/C-ImmSim/) was utilized to simulate the extent and type of immune response induced by MEV in humans [55]. The server simulation represents three distinct parts of the mammalian anatomy, including the bone marrow, thymus, and lymph. The three different intervals are 1, 84 and 16,833. Finally, parameters are configured to their default values in the software, while the simulation parameters are initialized with a random seed of 12,345. The number of simulations is set to 50, and each simulation consists of 1050 steps.

2.8.8. Optimization of codons and in silico cloning

The codon was optimized using JCAT (JAVA Codon adaptation tool) to obtain the optimized DNA sequence (http://www.Jcat.de/). RNAfold 2.4.18 (http://rna.tbi.univie.ac.at/cgibin/RNAWebSuite/RNAfold.cgi) was employed for predicting the secondary structure of RNA, ensuring efficient translation of MEV1 [56]. The plasmid's DNA sequence was acquired from the Plasmid Files, with pET-28a (+) selected as the vector. XHOI and *Bam*HI were selected as restriction enzyme sites, and the optimized DNA sequence was inserted into the multiple cloning site (MCS) region of the vector to achieve a comprehensive plasmid structure for further investigation.

3. Results

3.1. Selection of target antigens

The FASTA sequences of two strains were obtained from the NCBI database. The related proteins of the *K. pneumoniae* ST258 lineage were found from the database, namely OmpA (Accession no: KAA8836359.1), OmpC (Accession no: KAA8842888.1), OmpX (Accession no: AZI11103.1), OmpW (Accession no: KAA8838963.1), OmpK35 (Accession no: RLK86282.1), OmpK37 (Accession no: KAA8839221.1), pal (Accession no: KAA8836096.1), phosphoprotein PhoE (Accession no: KAA8835218.1), PmrB (Accession no: KAA8836139.1), LamB (Accession no: KLA41972.1), phoQ (Accession no: KAA8836485.1), capsule biosynthesis protein CapA

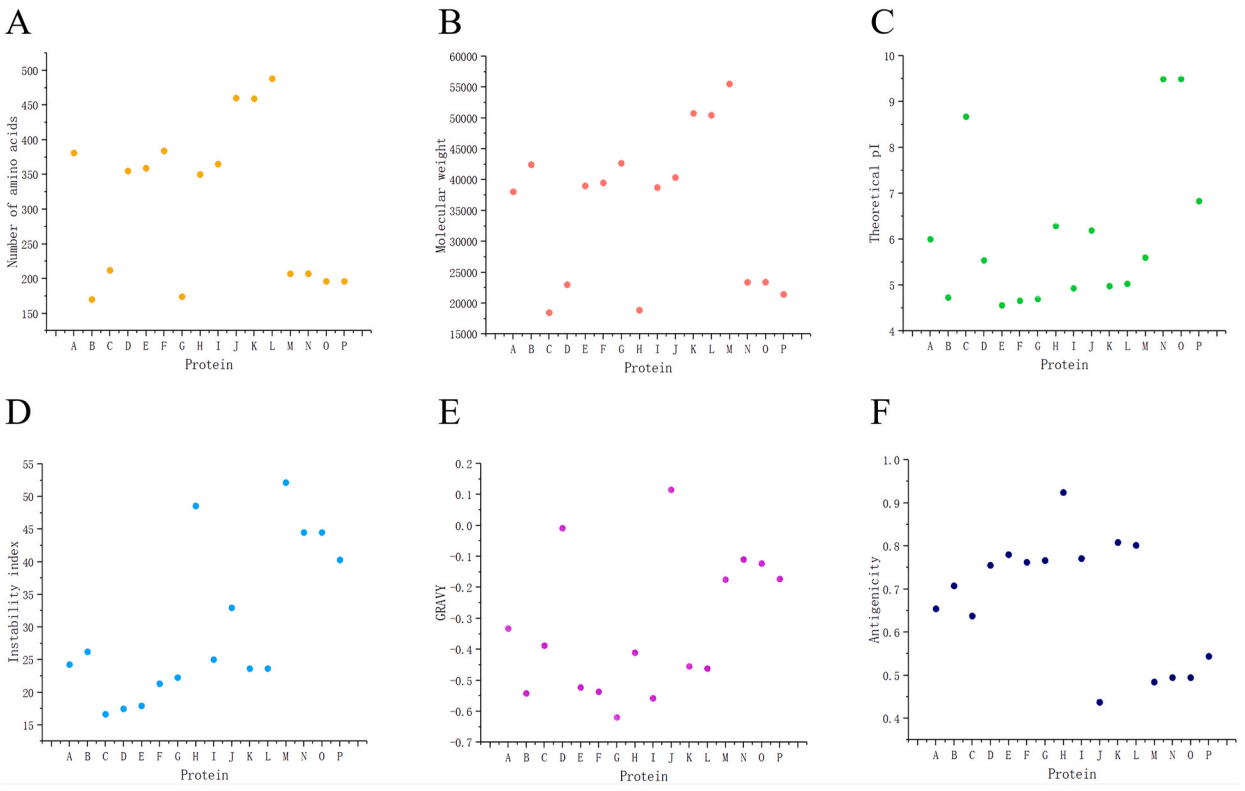

Fig. 2. The physicochemical properties of proteins of *K. pneumoniae.* (A) Number of amino acids of proteins. (B) The molecular weight of proteins. (C) The theoretical PI of proteins. (D) The instability index of proteins. (E) The GRAVY of proteins. (F) The antigenicity of proteins.

(Accession no: KLA39288.1), and LPS biosynthesis protein (Accession no: OCV26311.1). Similarly, the related proteins of the *K. pneumoniae* ST11 lineage were found from the database, namely OmpA (Accession no: UKA32865.1), OmpC (Accession no: UKA34288.1), OmpX (Accession no: OIK32342.1), OmpW (Accession no: UKA33110.1), OmpK35 (Accession no: UKA32840.1), OmpK37 (Accession no: UKA33312.1), pal (Accession no: UKA32605.1), phosphoporin PhoE (Accession no: UKA32078.1), PmrB (Accession no: UKA32649.1), LamB (Accession no: KEP95397.1), phoQ (Accession no: UKA32992.1), capsule biosynthesis protein CapA (Accession no: KEP95327.1), and LPS biosynthesis protein (Accession no: OCU75495.1). Using Jalview to compare protein sequences, we found that OmpA, OmpC, OmpX, OmpW, OmpK37, pal, phosphoporin PhoE, PmrB, phoQ, and LPS biosynthetic protein have 100% homology in ST258 and ST11 strains. Through physicochemical properties and antigenicity analysis, we selected proteins with highly conserved sequences (Fig. 2A and B), good stability (Fig. 2C and D), strong hydrophilicity (Fig. 2E), and high antigenicity (Fig. 2F) as candidate proteins. Next, it was found that OmpA, OmpC, OmpX, OmpW, and OmpK37 have no homology to human proteins. By observing the homology with other bacterial proteins, we found that OmpA and *Stenotrophomonas maltophilia* L1 β-lactamase are highly homologous to each other, with an E value of 3.55113. OmpC has the highest homology with *Serratia marcescens* Omp1, with an E value of 5.07943E-179. OmpX has the highest homology with *Elizabethkingia meningoseptica* GOB-5, with an E value of 6.52497. OmpW has the highest homology with *Pseudomonas aeruginosa* aadA13, with an E value of 3.61064. OmpK37 has the highest homology with *Serratia marcescens* Omp1, with an E value of 1.28368E-175. Through the analysis of biological activity, we found that OmpA belongs to the outer membrane OOP (TC 1.B.6) superfamily and probably serves as the mating receptor on recipient cells; OmpC belongs to Porin and is related to the mechanism of drug resistance-beta-Lactam resistance; OmpX also belongs to the outer membrane OOP (TC 1.B.6) superfamily and is the virulence-related outer membrane protein; the biological activity of OmpW is still in the exploratory stage; and Ompk37 has the porin activity, mainly involved in ion transport across the membrane. Finally, through the sequence comparison again, the target proteins have a certain similarity, especially the starting sequence of the proteins **(Supplementary Fig. 1).**

3.2. Prediction of target protein subcellular localization and signaling peptides

The results showed that the target proteins were transmembrane structures with different β-folding regions (Fig. 3A–E). In addition, all target proteins contained signal peptides. The 1–3 peptides of OmpA are the N-region of signal peptide Sec/SPI, the 4–18 peptides are the H-region of signal peptide Sec/SPI, the 19–21 peptides are the C-region of Sec/SPI, and the 22–24 peptides are the junctional region (Fig. 3F). The 1–4 peptides of OmpC are the N-region of signal peptide Sec/SPI, the 5–17 peptides are the H-region of signal peptide Sec/SPI, the 18–21 peptides are the C-region of Sec/SPI, and the 22–24 peptides are the junctional region (Fig. 3G). The 1–3 peptides of OmpX are the N-region of signal peptide Sec/SPI, the 4–18 peptides are the H-region of signal peptide Sec/SPI, the 19–24 peptides are the C-region of Sec/SPI, and the 24–26 peptides are the junctional region (Fig. 3H). The 1–3 peptides of OmpW are the N-region of signal peptide Sec/SPI, the 4–14 peptides are the H-region of signal peptide Sec/SPI, the 15–21 peptides are the C-region of Sec/SPI, and the 22–24 peptides are the junctional region (Fig. 3I). The 1–4 peptides of OmpK37 are the N-region of signal peptide Sec/SPI, the 5–16 peptides are the H-region of signal peptide Sec/SPI, the 17–21 peptides are the C-region of Sec/SPI, and the 21–24 peptides are the junctional region (Fig. 3J). Finally, 1–24 peptides of OmpA, 1–24 peptides of OmpC, 1–26 peptides of OmpX, 1–24 peptides of OmpW, and 1–24 peptides of OmpK37 are signal peptides.

3.3. Prediction of CTL cell epitopes

Sorted according to percentiles from small to large, OmpA (Fig. 4A) contains 10 CTL epitopes (YTDRIGSEAY, SPVFAGGVEW, AQAAPKDNTW, MLSLGVSYRF, HFTLKSDVLF, QAAPKDNTWY, TLKPEGQQAL, TLKSDVLFNF, AVTRDIATRL, QALDQLYTQL) after screening. Screened OmpC (Fig. 4B) contains 20 CTL epitopes (KYVDVGMTYY, YYDLDMGISF, TQNFEVVAQY, YYFNKNMSTY, YQFDDFNLPL, VKYVDVGMTY, MYAETRNMTF, NLPLRPSVAY, YVDVGMTYYF, ADAWTVGAKY, TSEKEGANSW, RYGDKDLVKY, GDTYTQTDVY, STYVDYKINL, NMTFYGNDSF, YGKVDGLHYF, TQITSELTGY, YAETRNMTFY, QSKGKDLYAY, ATDDIVALGL). The

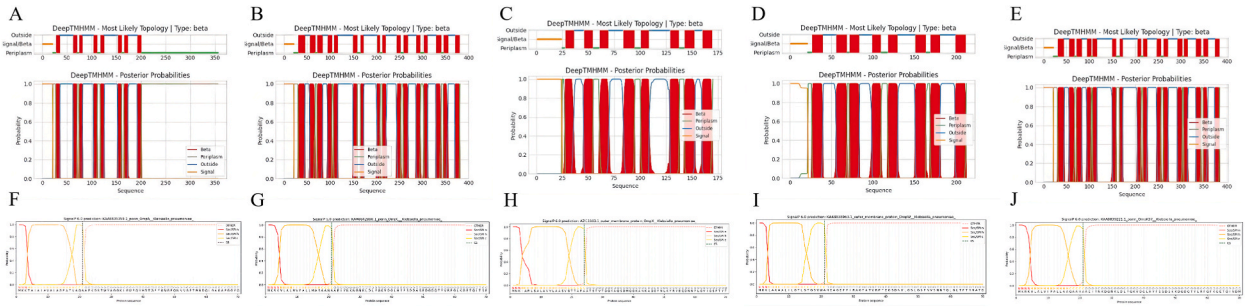

Fig. 3. (A) Subcellular localization of protein OmpA. (B) Subcellular localization of protein OmpC. (C) Subcellular localization of protein OmpX. (D) Subcellular localization of protein OmpW. (E) Subcellular localization of protein Ompk37. (F) The signal peptide sequence of OmpA. (G) The signal peptide sequence of OmpC. (H) The signal peptide sequence of OmpX. (I) The signal peptide sequence of OmpW. (J) The signal peptide sequence of Ompk37.

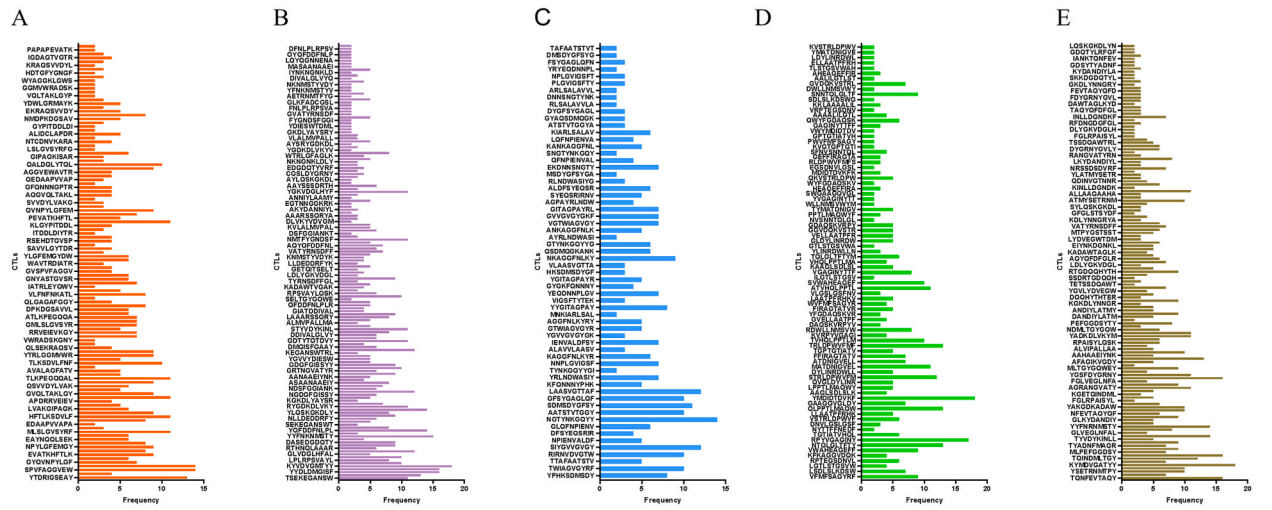

Fig. 4. The CTL epitopes are represented in longitudinal coordinates, and the epitopes' frequency in 27 alleles is represented in transverse coordinates. (A) The CTL epitopes of OmpA. (B) The CTL epitopes of OmpC. (C) The CTL epitopes of OmpX. (D) The CTL epitopes of OmpW. (E) The CTL epitopes of Ompk37.

screened OmpX (Fig. 4C) contains 8 CTL epitopes (NGTYNKGQYY, SIYGVVGVGY, LAASVGTTAF, SDMSDYGFSY, TWIAGVGYRF, RIRNVDVGTW, AATSTVTGGY, GFSYGAGLQF). The screened OmpW (Fig. 4D) contains 10 CTL epitopes (YMDIDTDVKF, RPYVGAGINY, NTQLGLTFTY, QLPPTLMAQW, TRLDPWVFMF, STRLDPWVFM, MATDNIGVEL, ATVHQLPPTL, TVHQLPPTLM, SVWAHEAGEF). The screened OmpK37 (Fig. 4E) contains 19 CTL epitopes (KYMDVGATYY, TQNFEVTAQY, RYADKDLVKY, YMDVGATYYF, VKYMDVGATY, YYFNRNMSTY, ADAWTAGLKY, TQINDMLTGY, AGRANGVATY, YGSFDYGRNY, YADKDLVKYM, STYVDYKINL, YGKVDGLHYF, YSETRNMTPY, QQHYTHTERY, STSYDFGMGI, YAKGDKADAW, DSKKDGDQTY, ATMYSETRNM).

3.4. Prediction of HTL cell epitopes

Sorted according to percentiles from small to large, OmpA (Fig. 5A) contains 7 HTL epitopes (IEVKGYKEVVTQPAA, SVVDYLVAKGIPAGK, KGNYASTGVSRSEHD, VVDYLVAKGIPAGKI, QSVVDYLVAKGIPAG, SKGNYASTGVSRSEH, EIEVKGYKEVVTQPA) after screening. OmpC (Fig. 5B) contains 2 HTL epitopes (DGLHYFSDDASEDGD, VDGLHYFSDDASEDG). OmpX (Fig. 5C) contains 7 HTL epitopes (NKGQYYGITAGPAYR, KGQYYGITAGPAYRL, YNKGQYYGITAGPAY, TTAFAATSTVTGGYA, GAGLQFNPIENVALD, GQYYGITAGPAYRLN, AGLQFNPIENVALDF). OmpW (Fig. 5D) contains 2 CTL epitopes (GEFFIRAGTATVRPT, AGEFFIRAGTATVRP).

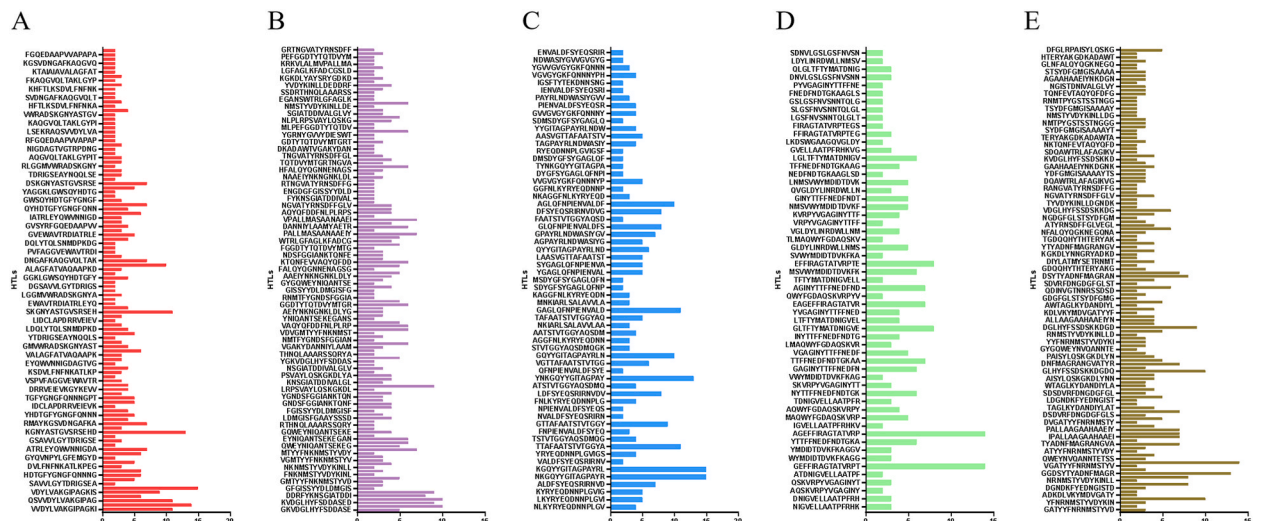

Fig. 5. The HTL epitopes are represented in longitudinal coordinates, and the epitopes' frequency in 27 alleles is represented in transverse coordinates. (A) The HTL epitopes of OmpA. (B) The HTL epitopes of OmpC. (C) The HTL epitopes of OmpX. (D) The HTL epitopes of OmpW. (E) The HTL epitopes of Ompk37.

OmpK37 (Fig. 5E) contains 4 CTL epitopes (GDSYTYADNFMAGRA, GGDSYTYADNFMAGR, ADNFMAGRANGVATY, GLHYFSSDSKKDGDQ).

3.5. Prediction of B cell epitopes

After analysis, OmpA has fifteen linear B cell epitopes; OmpC has nineteen linear B cell epitopes; OmpX has nine linear cell epitopes; OmpW has thirteen linear B cell epitopes, and Ompk37 has twenty-five linear B cell epitopes. After highly accurate predictions, the tertiary structures of these five proteins are barrel-shaped (Fig. 6A–E). After further analysis of the model quality, the Ramachandran plot of OmpA (Fig. 6F) shows that the model has 96.61% favorable regions, 3.39% generously allowed regions, and 0.00% outlier regions. The Ramachandran plot of OmpC (Fig. 6G) shows that the model has 95.25% favorable regions, 4.49% generously allowed regions, and 0.26% outlier regions. The Ramachandran plot of OmpX (Fig. 6H) shows that the model has 94.64% favorable regions, 4.17% generously allowed regions, and 1.19% outlier regions. The Ramachandran plot of OmpW (Fig. 6I) shows that the model has 97.62% favorable regions, 2.38% generously allowed regions, and 0.00% outlier regions. The Ramachandran plot of Ompk37 (Fig. 6J) shows that the model has 95.55% favorable regions, 3.40% generously allowed regions, and 1.05% outlier regions. After analysis, OmpA contains 3 conformational B cell epitopes, OmpX contains 2 conformational B cell epitopes, OmpW contains 1 conformational B cell epitope, and there are no conformational B cell epitopes in OmpC and Ompk37.

3.6. Selection of dominant cell epitopes and adjuvant

After another screening **(Table 1)**, we finally obtained 15 dominant CTL cell epitopes, 10 dominant HTL cell epitopes, 6 dominant linear B cell epitopes, and 2 dominant conformational B cell epitopes (Fig. 7A–B). The candidate adjuvant CTB (accession number: P01556) and LTA1 (accession number: P06717) were obtained from UniProt. After analysis, these two proteins are outer membrane proteins (Fig. 7C–D). The signal peptide sequences of CTB (Fig. 7E) and LTA1 (Fig. 7F) were 1–24 peptides and 1–24 peptides, respectively. Finally, we chose the 25–124 peptides of CTB and the 24–258 peptides of LTA1 as candidate adjuvants.

3.7. Analysis of population coverage of the T epitopes

The average hit represents the mean number of epitope hits/HLA combinations recognized by the population, while PC90 indicates the minimum number of epitope hits/HLA combinations recognized by 90% of the population. Following analysis, the population coverage of HLA-I molecules for the T epitopes was 98.55% with an average hit of 14.03 and PC90 of 5.42 (Fig. 8A). The population coverage of HLA-II molecules reached 99.48%, accompanied by an average hit of 15.36 and a PC90 value of 6.78 (Fig. 8B). The overall population coverage was 99.99%, the average hit was 29.39, and PC90 was 16.5 (Fig. 8C).

3.8. Construction of multi-epitope vaccines

After construction, we successfully generated MEV1 incorporating CTB as an adjuvant and MEV2 incorporating LTA1 as an adjuvant. A schematic representation illustrating the composition of the developed vaccine is depicted in Fig. 9.

3.8.1. Analysis of the physicochemical properties of vaccines

The results demonstrated that MEV1 exhibited an antigenicity value of 1.021, encompassing a sequence of 743 amino acids. The

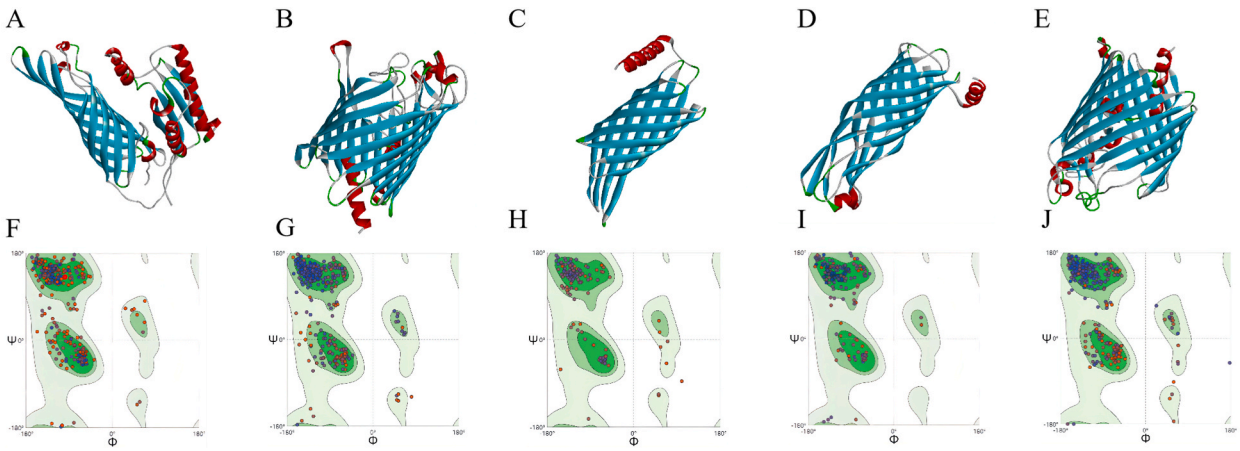

Fig. 6. (A) The tertiary structure of OmpA. (B) The tertiary structure of OmpC. (C) The tertiary structure of OmpX. (D) The tertiary structure of OmpW. (E) The tertiary structure of Ompk37. (F) The ramachandran plot of OmpA. (G) The ramachandran plot of OmpC. (H) The ramachandran plot of OmpX. (I) The ramachandran plot of OmpW. (J) The ramachandran plot of Ompk37.

Table 1
The dominant cell epitopes.

	OmpA		OmpC		OmpX		OmpW OmpK37			
	epitopes	Antigenicity	epitopes	Antigenicity	epitopes	Antigenicity	epitopes	Antigenicity	epitopes	Antigenicity
CTL s	HFTLKSDVLF	1.0905	YYFNKNMSTY	0.4165	TWIAGVGYRF	0.9887	ATVHQLPPTL	0.7762	TQNFEVTAQY	1.3376
	TLKSDVLFNF	0.8133	YQFDDFNLPL	0.7081					YYFNRNMSTY	0.4028
	AVTRDIATRL	0.7188	VKYVDVGMTY	0.6866					AGRANGVATY	1.2091
			YAETRNMTFY	0.4133					QQHYTHTERY	0.4925
			QSKGKDLYAY	1.2379					STSYDFGMGI	1.0087
HTL s	IEVKGYKEVVTQPAA	0.7095	DGLHYFSDDASEDGD	0.4244	NKGQYYGITAGPAYR	0.5335	–	–	GDSYTYADNFMAGRA	0.7085
	SKGNYASTGVSRSEH	1.0067	VDGLHYFSDDASEDG	0.4336	KGQYYGITAGPAYRL	0.954	–	–	ADNFMAGRANGVATY	0.7698
					GAGLQFNPIENVALD	1.0101	–	–		
					AGLQFNPIENVALDF	0.8443	–	–		
LB s	GDAGTVGTRPDNGMLS	1.4052	FALQYQGNNENAGSGE	1.9484	GKANKAGGFNLKYRYE	1.6162	TATVRPTEGSDNVLGS	1.4038	NFEVTAQYQFDFGLRP	1.8176
			EYNIQANTSEKEGANS	2.0264					GSTSSTNGGGIANKTQ	2.0643
CB s	DTGFYGNGFQNNNGPTRG RAYKGSVDNGAVRADSKG NYASTGVSRSEHDTGVNIG DAGTVGTRP	1.0512	–	–	–	–	GSDNVLGSLGSTGPTGT DFNDTGKAAGLSDSKDD KKAGGVDQKS	1.2058	–	–

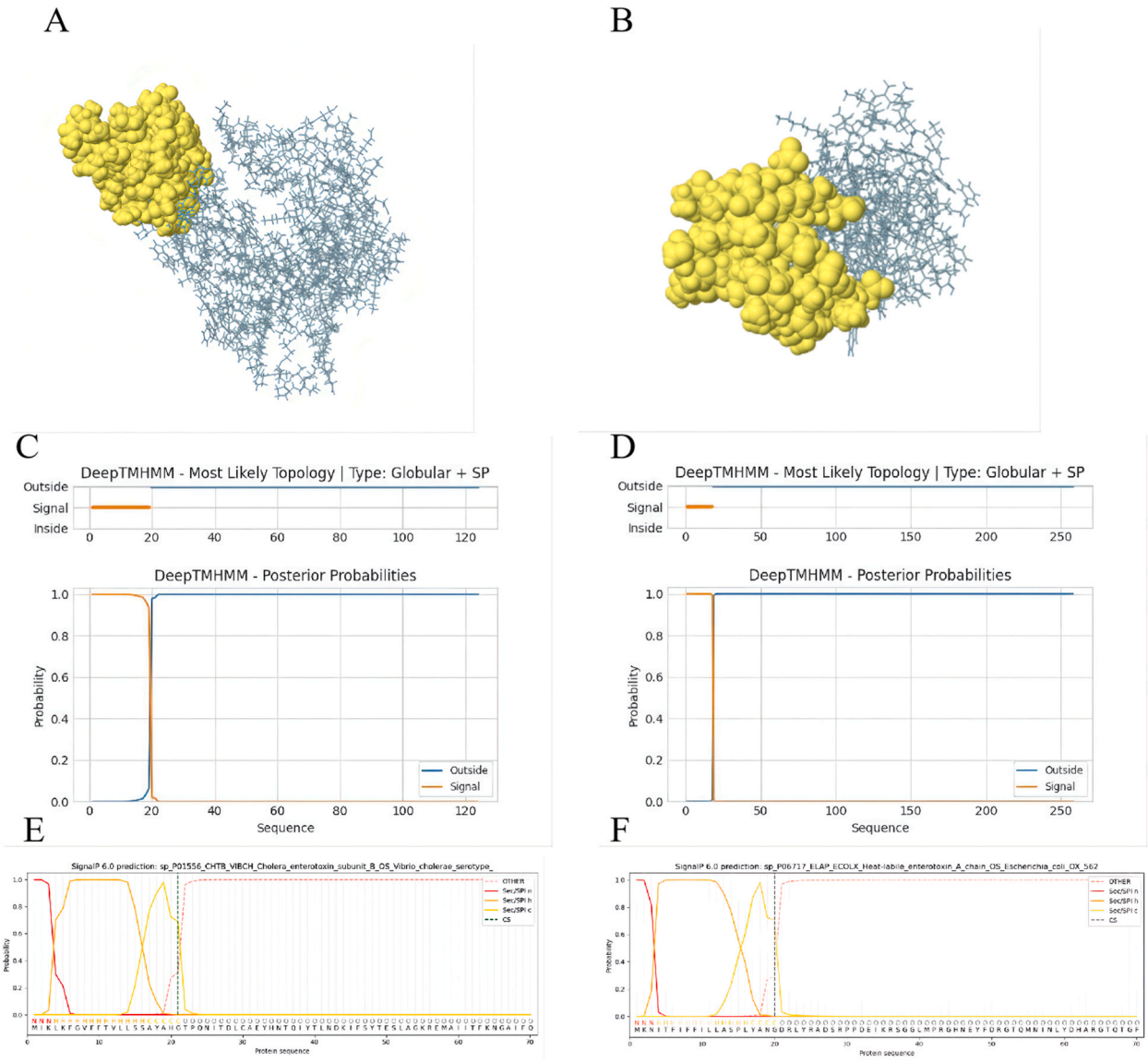

Fig. 7. (A) B-cell conformational epitopes of OmpA (A:D41, A:T42, A:G43, A:F44, A:Y45, A:G46, A:N47, A:G48, A:F49, A:Q50, A:N51, A:N52, A:N53, A:G54, A:P55, A:T56, A:R57, A:G85, A:R86, A:A88, A:Y89, A:K90, A:G91, A:S92, A:V93, A:D94, A:N95, A:G96, A:A97, A:V127, A:R129, A:A130, A:D131, A:S132, A:K133, A:G134, A:N135, A:Y136, A:A137, A:S138, A:T139, A:G140, A:V141, A:S142, A:R143, A:S144, A:E145, A:H146, A:D147, A:T148, A:G149, A:V150, A:N177, A:I178, A:G179, A:D180, A:A181, A:G182, A:T183, A:V184, A:G185, A:T186, A:R187, A:P188). (B) B-cell conformational epitopes of OmpA (A:G41, A:S42, A:D43, A:N44, A:V45, A:L46, A:G47, A:S48, A:L49, A:G50, A:S51, A:T88, A:G89, A:P90, A:T91, A:G92, A:T93, A:D134, A:F135, A:N136, A:D137, A:T138, A:G139, A:K140, A:A141, A:A142, A:G143, A:L144, A:S145, A:D146, A:S148, A:K150, A:D151, A:D183, A:K185, A:K187, A:A188, A:G189, A:G190, A:V191, A:D192, A:Q193, A:K194, A:S196). (C) Subcellular localization of CTB. (D) Subcellular localization of LTA1. (E) The signal peptide of CTB. (F) The signal peptide of LTA1.

atomic weight was determined to be 78914.9 KD, while the theoretical isoelectric point (pI) was calculated as 8.63. Its molecular formula was identified as $C_{3498}H_{5272}N_{962}O_{1106}S_{13}$, with an instability index of 25.23 and an aliphatic index of 52.81. Moreover, the grand average of hydropathicity (GRAVY) indicated a value of −0.618, and its solubility reached a level of 0.798706.

In addition, the antigenicity of MEV2 was 0.9541, including 878 amino acids. And the weight of the atom was 94915.02 KD, the theoretical PI was 8.01, the formula was $C_{4204}H_{6285}N_{1177}O_{1324}S_{13}$, instability index was 28.48, the aliphatic index was 52.89, the GRAVY was −0.706 and the solubility was 0.860296. Finally, a more intuitive reflection of the hydrophobicity map of the MEV1 is hydrophilic protein (Fig. 10A). Likewise, MEV2 is also a hydrophilic protein (Fig. 10B). Based on comprehensive analysis, it can be concluded that MEV1 is more suitable as a potential vaccine candidate against *K. pneumoniae* ST258 and ST11 for the next analysis.

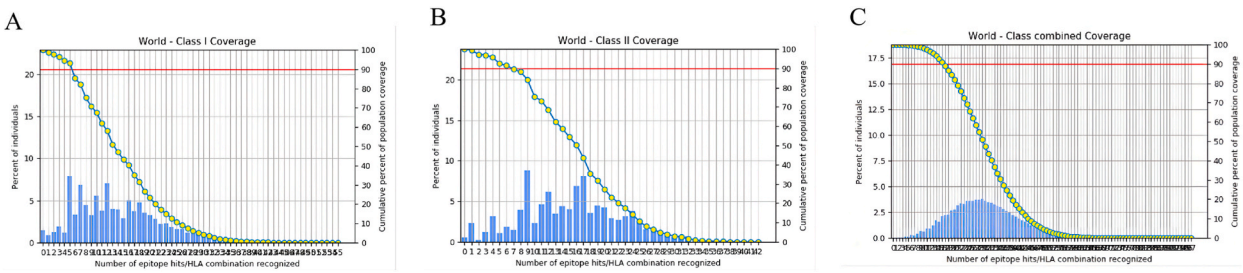

Fig. 8. (A) Population coverage of dominant CTL cell epitopes. (B) Population coverage of dominant HTL cell epitopes. (C) Population coverage of dominant T cell epitopes.

Fig. 9. Schematic diagram of construction of multi-epitope vaccine.

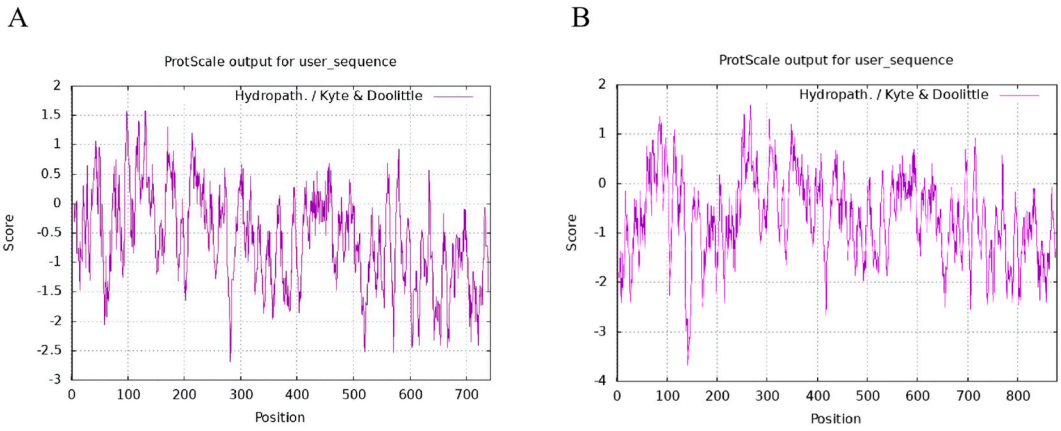

Fig. 10. (A) Analysis of hydrophobicity of cholera toxin B. (B) Analysis of hydrophobicity of LTA1.

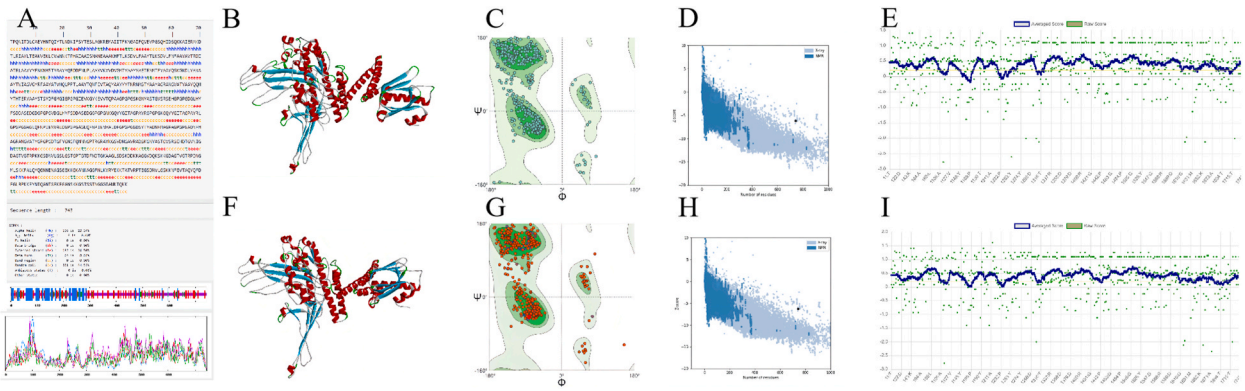

Fig. 11. (A) The secondary structure of MEV1. (B) The original tertiary structure of MEV1 is predicted. (C) A ramachandran plot of the original tertiary structure of MEV1. (D) A z-score diagram of the original tertiary structure of MEV1. (E) The original three-level structure of the ERRAT graph for MEV1. (F) The refined tertiary structure of MEV1. (G) A ramachandran plot of the refined tertiary structure of MEV1. (H) A z-score diagram of the refined tertiary structure of MEV1. (I) The refined three-level structure of the ERRAT graph for MEV1.

3.8.2. Prediction, refinement, and validation of 3D vaccine construct

In the secondary structure prediction map (Fig. 11A), it is observed that α-helices accounted for 22.34%, extended strand for 24.5%, β-turn for 8.61%, and random coil for 44.55%. In addition, in the 3D structure before and after optimization (Fig. 11B–F), a similar trend is observed with extended strands and random coils occupying a larger proportion of columns. In the pre-optimization evaluation of the 3D structure, the Ramachandran plot indicated that 93.79% of regions were favorable, 5.54% were generously allowed, and only 0.67% fell into the outlier region (Fig. 11C). The Z-score was −6.18 (Fig. 11D), while a minimum of 80% of amino acids in ERRAT predicted results scored ≥0.2 in the 3D/1D profile (Fig. 11E). In the evaluation of the 3D structure following optimization, the Ramachandran plot revealed that 93.93% of regions were favorable, while 5.67% fell within generously allowed regions and only 0.40% were classified as outliers (Fig. 11G). The Z-score was determined to be −6.32 (Fig. 11H). Moreover, a minimum of 80% of amino acids in the ERRAT predicted results achieved a score greater than or equal to 0.2 in the comprehensive analysis combining both three-dimensional and one-dimensional profiles (Fig. 11I).

3.8.3. Disulphide bridging for vaccine stability

After disulfide structure analysis, a total of 77 pairs of residues were used to identify the disulfide-modified regions (Fig. 12). By calculating the energy fraction and the angle of χ3,4 residue pairs were selected as disulfide regions. For MET101-ALA107 residual pairs, the energy score was 2.06 kcal/mol and the χ3 angle value was −63.76°. For GLY219-ALA246 residual pairs, the energy score was 2.03 kcal/mol and the χ3 angle value was −81.09°. Similarly, for GLY368-LYS595 residual pairs, the energy score was 1.95 kcal/mol and the χ3 angle value was −65.67°. Lastly, in the case of the LYS725-ILE736 pair of residues, the score of the energy was 2.14 kcal/mol and the value of the angle of χ3 was −79.25°.

Fig. 12. A schematic diagram of the structure of MEV1 after disulfidation.

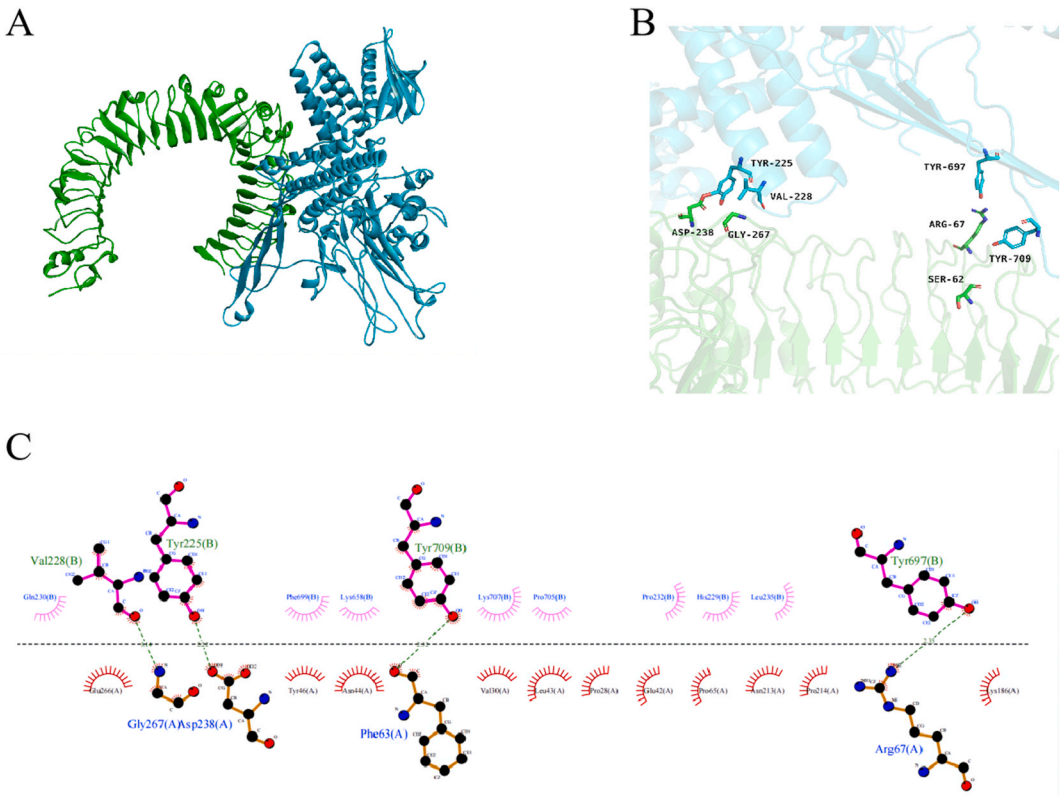

Fig. 13. (A) The molecular docking structure of MEV1 and TLR4. As illustrated in the figure, "blue" stands for the MEV1, and "green" stands for the TLR4. (B) The interaction residues between MEV1 and TLR4 were analyzed by PyMol. (C) Ligplus shows a two-dimensional analysis (green dotted lines, hydrogen bonds) of the relative forces of TLR4 and MEV1.

3.8.4. Molecular docking with TLR4

TLR4 (PDB ID: 4G8A) was obtained from the PDB database. Following docking analysis (Fig. 13A), the original MEV1 exhibited a docking score of −317.30 and a ligand RMSD of 67.83 Å. After model refinement, MEV1 displayed an improved docking score of −336.63 and a ligand RMSD of 172.00 Å. Similarly, after desulfurization, MEV1 maintained a docking score of −336.63 with a slightly reduced ligand RMSD value of 171.98 Å. By investigating the molecular interaction between TLR4 and MEV1 (Fig. 13B), it has been observed that the refined model exhibits a comparable molecular interaction force to that of the disulfide model. Consequently, it can be preliminarily inferred that sulfidation has minimal impact on the alteration of molecular structure. Regarding the interaction between MEV1 and TLR4 (Fig. 13C), Ligplus analysis revealed the presence of five pairs of hydrogen bonds between these entities.

3.8.5. Molecular dynamics simulation

The analysis revealed that the deformability map exhibited a minimal residual distortion in the complex (Fig. 14A). Furthermore, the deviation of the B-factor value calculated by NMA was less than that of the complex (Fig. 14B). In addition, the eigenvalue of the complex was $3.48e^{-06}$ (Fig. 14C). In the variance graph (Fig. 14D), individual variance showed a decreasing trend in each continuous pattern, while cumulative variance showed an increasing trend. Overall iMODS showed low deformability and stability of the complex. In addition, the stability of the complex was more directly reflected in the MD simulation at 100 ns. At the beginning of the simulation, the RMSD value of the complex increased sharply (Fig. 14E). During the remaining simulation time, the structure deviation of the complex stabilized at the RMSD value of nearly 0.8 nm after 50 ns. During MD dynamics, the root means square wave (RMSF) analysis of the complex represented the stability of the interface between MEV1 and TLR4 (Fig. 14F). The main atom of the residue in the complex was calculated by RMSF, which showed that the two chains of the complex can be in the fluctuating range (<1 nm). The hydrogen bond between MEV1 and TLR4 in the complex was calculated, and the stability of the interface was defined in the MD simulation. The results (Fig. 14G) showed that there were 5 hydrogen bonds at the interface of 0–30 ns and 10 hydrogen bonds at the interface of 30–100 ns. The compactness of MEV1-TLR4 was determined by enumerating the Rg data of the complex (Fig. 14H). The results demonstrated that the rotation fluctuation of the backbone atom was relatively stable, and varied from 4.30 nm to 4.45 nm. Finally, the average binding energy of the complex was found to be −230.7407 kJ mol^{-1} using the MMGBSA tool. Further visualizations of these results can be found in Supplementary Fig. 2.

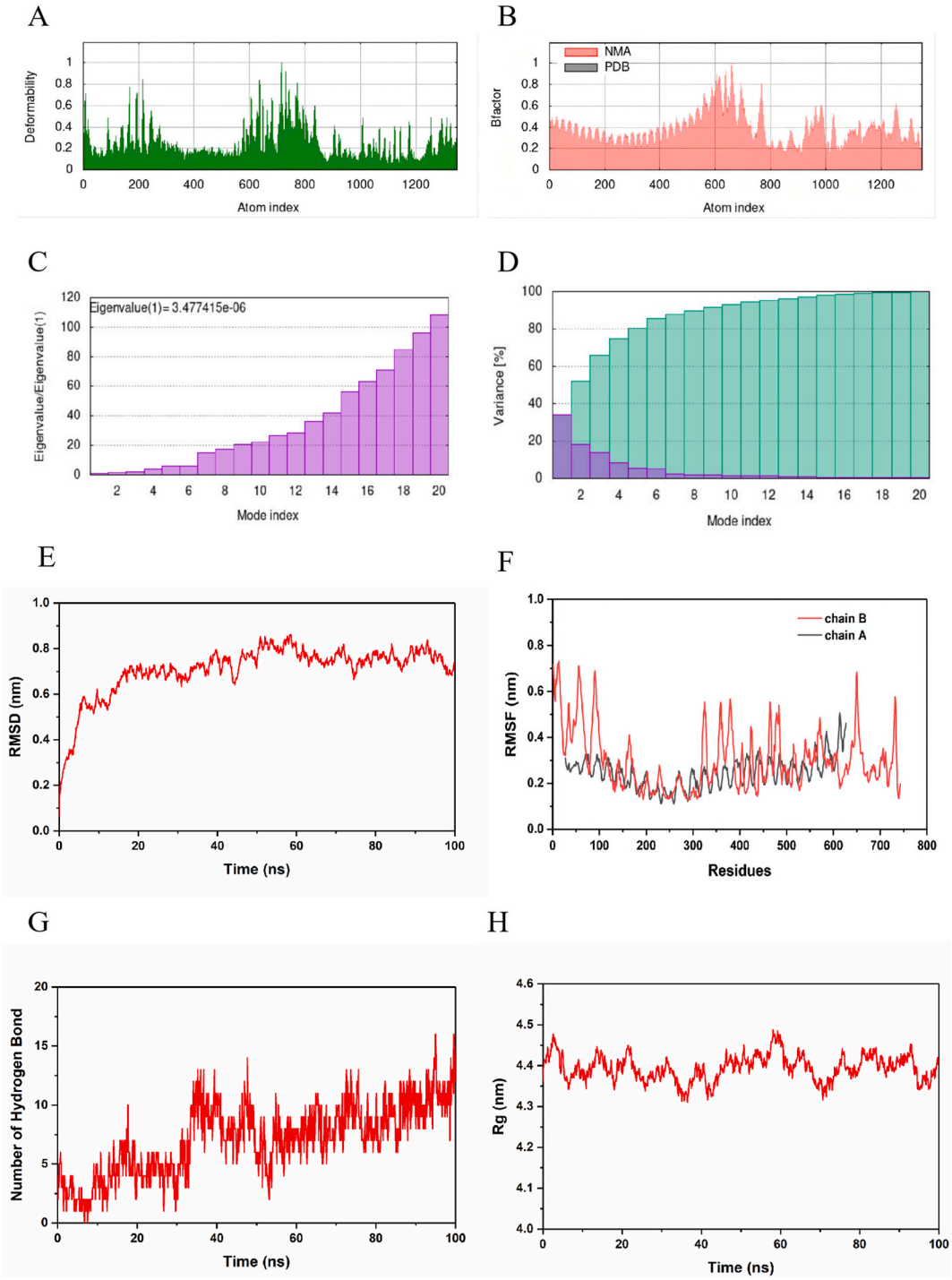

Fig. 14. (A) The deformability map of MEV1-TLR4 analyzed by iMODS. (B) The B-factor value map of MEV1-TLR4 analyzed by iMODS. (C) The eigenvalue map of MEV1-TLR4 analyzed by iMODS. (D) The variance graph of MEV1-TLR4 analyzed by iMODS. (E) The RMSD diagram of the complex analyzed by Gromacs 2021.3. (F) The RMSF diagram of the complex analyzed by Gromacs 2021.3. (G) The number of total hydrogen bonds diagram of the complex analyzed by Gromacs 2021.3. (H) The radius of gyration (Rg) diagram of the complex analyzed by Gromacs 2021.3.

3.8.6. Principal component analysis

The MEV1-TLR4 complex (Fig. 15) was simulated with 100ns trajectories and analyzed by PCA. PCA projects data into two dimensions (2D) through its coordinates in principal component 1 (PC1) and principal component 2 (PC2). PC1 of MEV1-TLR4 was distributed at -10-22.5 nm and PC2 of MEV1-TLR4 was distributed at -10-12.5 nm. Notably, the constructive distribution displayed

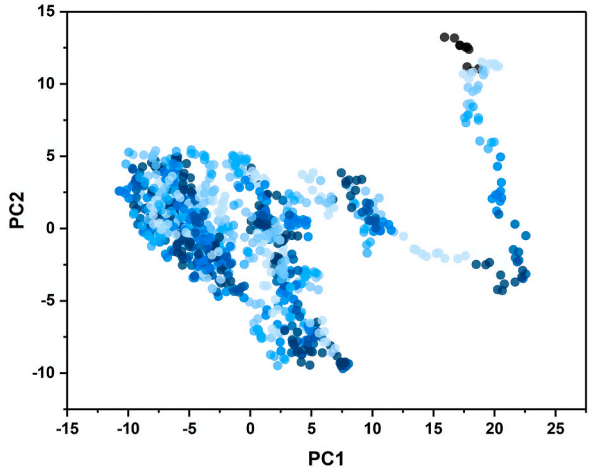

Fig. 15. Principal component analysis of MEV1-TLR4.

minimal fluctuations, indicating robust stability in the docking interaction between MEV1 and TLR4.

3.8.7. Immune simulation

After immunomodulation, the antibody levels reached a certain level after three doses of vaccine injection, specifically IgM + IgG (Fig. 16A). Additionally, the injection of the vaccine also caused a series of changes in cytokines produced by the host, mainly the increase of IFN-γ (Fig. 16B). Regarding T cells (Fig. 16C) and B cells (Fig. 16D), which were mainly involved in adaptive immunity, their levels gradually increased to reach a stable high point. Conversely, dendritic cells (Fig. 16E) and macrophages (Fig. 16F), exhibited minimal fluctuations and consistently maintained elevated levels throughout.

3.8.8. Optimization of codons and in silico cloning

The optimized codon sequence consisted of 2229 amino acids, with a codon adaptation index (CAI) score of 1 and a GC content of 51.77% (Fig. 17A). The free energy of the thermodynamic ensemble was −717.12 kcal/mol. The frequency of the MFE structure in the ensemble was 0.00% (Fig. 17B). The ensemble diversity was 527.98. The optimized codon sequence (Fig. 17C) was inserted into pET-28 (+) and the 7564bp base sequence was obtained.

4. Discussion

K. pneumoniae, a common commensal bacterium in the gut, can cause various infections when it translocates from the gut to other sites such as urinary or respiratory tracts and even bloodstream [57]. If not promptly diagnosed and treated, it can easily invade the bloodstream and lead to severe septic shock, posing a life-threatening condition for patients. In recent years, there has been an alarming rise in extensively drug-resistant *K. pneumoniae* (XDR-KP), which significantly jeopardizes clinical anti-infective therapies. Furthermore, despite the recent advancements in β-lactam antibiotics and β-lactam inhibitors like ceftazidime-avibactam (CZA) combination therapy for *K. pneumoniae*, there has been a growing emergence of CZA-resistant *K. pneumoniae* isolates [58]. Therefore, it is very important to design a vaccine to prevent the disease early and realize mass immunity early. Research on prophylactic vaccines holds great potential in reducing antibiotic usage, curtailing the rise and dissemination of antimicrobial resistance (AMR), lowering the incidence rates of both susceptible and resistant infections, mitigating the severity of life-threatening illnesses, minimizing post-infection complications, and alleviating healthcare costs. MEV is constructed based on cell epitopes. Reverse vaccinology, a highly qualified genome-based approach, empowers experts to comprehensively explore the antigenic repertoire by leveraging the genomic sequences of specific organisms. By utilizing expressed genome sequences, reverse vaccinology facilitates the identification of potent vaccine candidates. This approach facilitates the production of vaccines that have posed challenges in manufacturing during the past decade. Therefore, reverse vaccinology has the potential to discover vaccines that can be used to improve the quality of existing vaccines. By employing immuno-informatics methodology for early-stage vaccine evaluation, we can efficiently select candidate vaccines with superior antigenicity, stability, and solubility as the candidate vaccine, resulting in significant savings in human resources, materials, and finances. In summary, it is a favorable choice for developing a vaccine using the method. Therefore, this study primarily revolves around *K. pneumoniae*, which often causes many kinds of hospital infection. The reverse vaccinology approach is employed to construct the MEV, which selectively targets highly antigenic, hydrophilic, stable, non-sensitizing and non-homologous proteins from humans such as OmpA, OmpC, OmpX, OmpW, and Ompk37. Bacterial transmembrane and secretory proteins are readily recognized by the host, thereby eliciting an immune response in the host, which is an important step in the selection of candidate proteins [59]. We analyzed five proteins, including OmpA, OmpC, OmpX, OmpW, and OmpK37. These five proteins are transmembrane proteins predominantly located on the outer side of the membrane. OmpA belongs to the outer membrane OOP (TC 1.B. 6) superfamily, OmpC is related to the mechanism of drug resistance-lactam resistance. OmpX also belongs to the outer membrane OOP

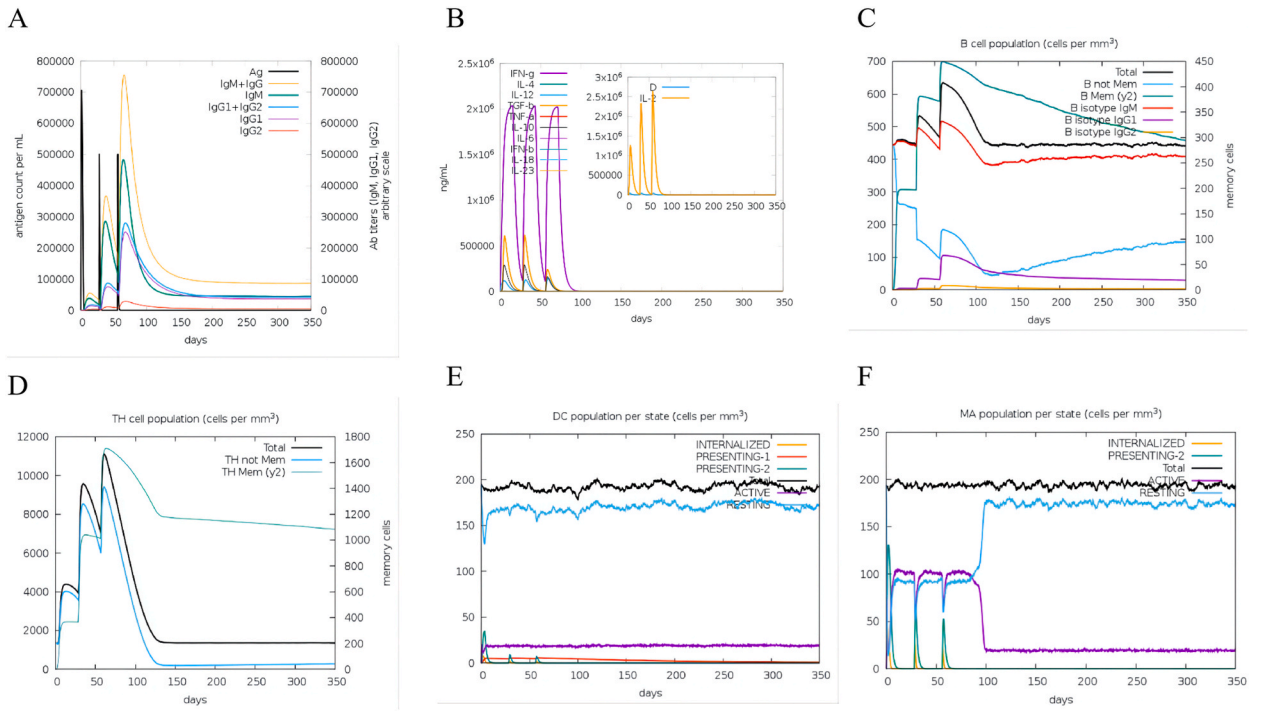

Fig. 16. Results of immune simulation of MEV1. (A) After three injections, antigen and antibody levels were measured. (B) After three injections, cytokine levels were measured. (C) Level of B cells after three injections. (D) Level of TH cells after three injections. (E) Level of DC cells after three injections. (F) Level of macrophage after three injections.

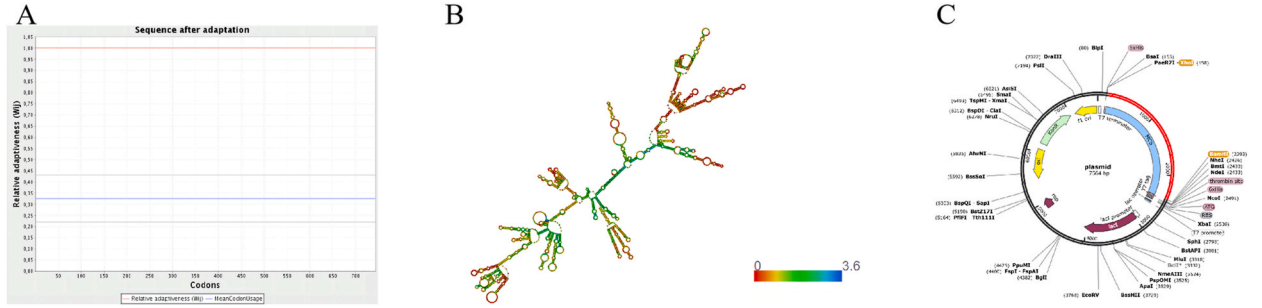

Fig. 17. (A) The optimized codon adaptation. (B) The optimized RNA secondary structure. (C) The recombinant plasmid was constructed with pET-28 (+) vector.

(TC 1.B. 6) superfamily and is a virulence-related outer membrane protein. The biological activity of OmpW is currently under investigation. OmpK37 exhibits pore protein activity and primarily contributes to ion transmembrane transport. In addition, signal peptides play an important role in protein secretion, these peptide sequences are cleaved from the mature protein by signal peptidase I during the late stage of the secretion process [60]. After the forecast, 1–24 peptides of OmpA, 1–24 peptides of OmpC, 1–26 peptides of OmpX, 1–24 peptides of OmpW, and 1–24 peptides of OmpK37 are signal peptides. Finally, predicted signal peptide sequences are not considered cell epitopes.

It is important to note that the predicted signal peptide sequences do not possess characteristics indicative of cell epitopes. MHC molecules, known as human leukocyte antigens (HLAs), exhibit high polymorphism in humans, with varying frequencies of different HLA alleles observed among ethnic groups [61]. CTL epitopes are involved in the development of long-lasting cellular immunity and can remove circulating viruses as well as virus-infected cells [62]. After analysis, we eventually obtained 15 dominant CTL cell epitopes. Whereas, HTL epitopes are recognized by T cells, triggering an adaptive immune response [63]. The analysis used alleles with a high frequency in the population, we eventually obtained 10 dominant HTL cell epitopes. Upon calculating the population coverage rate, the population coverage of HLA-I molecules for the T epitopes was 98.55%, the population coverage of HLA-II molecules was 99.48%, and the overall population coverage was 99.99%. Linear B-cell epitopes are effective antigenic peptide sequences for stimulating B-cell immune responses [64]. Most B-cell epitopes are discontinuous, and these conformational B-cell epitopes represent more

than 90% of functional B-cell epitopes [65]. Linear B cell epitopes were used in conjunction with conformational B cell epitopes to maximize the humoral immune response by the construct [66]. Ultimately, we eventually obtained 6 dominant linear B cell epitopes and two conformational B cell epitopes.

For the selection of dominant epitopes, it is crucial to identify non-allergenic and highly antigenic epitopes that can induce a robust immune response in the host without triggering anaphylaxis. In terms of linkers connecting different epitopes, we have opted for a rigid linker to ensure optimal connectivity. Specifically, AAY linkers can increase the immunogenicity of the MEV [67]. Furthermore, the GPGPG linkers are capable of eliciting $CD4^+$ T cell responses [68]. The KK linkers help to maintain the separate immunogenic properties of the MEV [69]. The EAAAK linkers provide an α-helix forming structure that increases stability, maintains a constant distance, and maintains the independent function of domains [70]. In terms of adjuvant selection, we opted for CTB and LTA1, which can trigger mucosal adjuvant, for comparison. In particular, CTB was a mucosal immunomodulatory protein that induced robust mucosal and systemic antibody responses [71]. After construction, both vaccine proteins were stable, hydrophilic, and highly soluble proteins. However, MEV1 was more antigenic and more suitable as a candidate vaccine. The antigenicity of MEV1 was 1.021, including 743 amino acids, the weight of the atom was 78914.9 KD, the theoretical pI was 8.63, the formula was $C_{3498}H_{5272}N_{962}O_{1106}S_{13}$, instability index was 25.23, the aliphatic index was 52.81, a grand average of hydropathicity (GRAVY) was −0.618 and the solubility was 0.798706. High antigenicity indicated that the vaccine could activate the immune response; the weight of the atom was less than 110 KD, indicating the weight of the vaccine was fair and suitable for the preparation of the vaccine [72]; the pI of the vaccine protein was slightly alkaline, indicating the stable interaction inside the human body; the instability index indicated that the protein was stable and represented the protein will be stable in vitro condition; the high aliphatic index indicated the good thermostable of protein; the hydrophilic index was negative and the solubility was higher than the threshold, which indicated that the protein was hydrophilic and soluble during its expression in *E. coli.* Thus, our data showed that the selected linkers and their adjuvant were appropriate, and the resulting epitopes could be presented in the host immune system.

By predicting the secondary structure of proteins, it was observed that a significant proportion of extended strands and random coils were present, indicating facile epitope formation [73]. The Z-score graph showed the average mass fraction of the input structure. Ramachandra's diagram was used to evaluate the energy disallowed and allowed dihedral angles of amino acid residues phi (φ) and psi (ψ). In addition, the ERRAT server was used to evaluate non-bond atom-atom interactions. By predicting the tertiary structure of the protein, the refined Z-score diagram and the Ramachandran plot showed higher accuracy of the model. To increase the stability of the MEV1, we selected 4 pairs of residual pairs for disulfide, further improving the structure of the vaccine.

Toll-like receptor 4 (TLR4) is a Gram-negative receptor protein that specifically binds to pathogen ligands [74]. Molecular docking, a widely used computer simulation method, serves as a strategic tool for vaccine design by exploring the binding affinity with proteins. By simulating TLR4 binding to the MEV1, it is possible to estimate the stability of transport in humans. The results suggested that there was a stable interaction between MEV1 and TLR4, which contributed to the enhancement of the immune response. In addition, the physical movement and stability of the docking complexes were evaluated by MDs. The lower deformation ability, lower B-factor value, and lower eigenvalue indicated that the composite was not easy to deform and its structure was relatively stable [75]. In addition, the smaller fluctuations of RMSD value, RMSF value, Rg data, and average binding energy showed the structural stability of the complex [76]. On the contrary, the increase in hydrogen bonds represented the stabilization of the interface between the MEV1 and TLR4 in the complex. Finally, it was confirmed that the MEV1-TLR4 complex had low deformability and remained stable.

In the context of immune simulation, it is evident that following vaccine administration, there is a notable increase in IgM and IgG levels. IgM mainly provides a rapid immune response and participates in tissue homeostasis, while IgG is a persistent high-affinity antibody with a long duration of action [77]. Moreover, the changes in cytokines were also observed in the course of immunomodulation, mainly the increase of IFN-γ. IFN-γ is mainly involved in the activation of APCs (macrophages, dendritic cells, and B cells), inducing the increased expression of class-II MHC and costimulatory molecules on the surface of APCs and enhancing the antigen-presenting function of APCs [78].

Evaluating the efficacy of cloning is a crucial step following its construction. After optimizing the sequence structure of the vaccine, the GC content was 51.77, while achieving a CAI value of 1. It is essential for the GC content to fall within an optimal range of 30–70% to ensure efficient expression of MEV1 in human hosts [79]. In addition, the optimal CAI value typically ranges from 0.8 to 1, with a CAI value of 1, indicating that the vaccine can be expressed to the highest degree [80]. Subsequently, upon inserting the optimized codon into pET-28 (+), we successfully obtained the complete plasmid, confirming that *E. coli* can express this vaccine. In conclusion, these results suggest that successful cloning of this vaccine in host organisms has been achieved, thereby laying a solid foundation for further experiments.

Funding information

This work was funded by the Wenzhou Science and Technology Bureau (Y2020990), and the Key Laboratory of Clinical Laboratory Diagnosis and Translational Research of Zhejiang Province (2022E10022).

Ethics approval and consent to participate

Not applicable.

Consent for publication

Not applicable.

Data availability statement

Data included in article/supplementary material/referenced in article. There are no restrictions on data availability.

Ethics declarations

Review and/or approval by an ethics committee was not needed for this study because the data in this paper is from the database, not including patient data.

CRediT authorship contribution statement

Min Li: Writing – original draft. **Mingkai Yu:** Software. **Yigang Yuan:** Software. **Danyang Li:** Methodology. **Daijiao Ye:** Software. **Min Zhao:** Software. **Zihan Lin:** Software. **Liuzhi Shi:** Writing – review & editing.

Declaration of competing interest

The authors declare that they have no known competing financial interests or personal relationships that could have appeared to influence the work reported in this paper.

Acknowledgements

The authors are thankful to the UniProt database and PDB library.

Appendix A. Supplementary data

Supplementary data to this article can be found online at https://doi.org/10.1016/j.heliyon.2024.e27417.

References

[1] L.P.P. Patro, T. Rathinavelan, Targeting the sugary Armor of Klebsiella species, Front. Cell. Infect. Microbiol. 9 (2019) 367.
[2] Antimicrobial Resistance Collaborators, Global burden of bacterial antimicrobial resistance in 2019: a systematic analysis, Lancet 399 (10325) (2022) 629–655.
[3] J.E. Choby, J. Howard-Anderson, D.S. Weiss, Hypervirulent Klebsiella pneumoniae - clinical and molecular perspectives, J. Intern. Med. 287 (3) (2020) 283–300.
[4] T.A. Russo, R. Olson, C.T. Fang, et al., Identification of Biomarkers for Differentiation of hypervirulent Klebsiella pneumoniae from classical K. pneumoniae, J. Clin. Microbiol. 56 (9) (2018) e00776-18.
[5] M. Kim, J.R. Yoo, H. Oh, Y.R. Kim, K.H. Lee, S.T. Heo, The first case of abdominal mycotic aneurysm caused by K1 hypervirulent Klebsiella pneumoniae in a healthy adult, Acute Crit Care 36 (4) (2021) 390–394.
[6] L. Shi, J. Feng, Z. Zhan, et al., Comparative analysis of blaKPC-2- and rmtB-carrying IncFII-family pKPC-LK30/pHN7A8 hybrid plasmids from Klebsiella pneumoniae CG258 strains disseminated among multiple Chinese hospitals, Infect. Drug Resist. 11 (2018) 1783–1793.
[7] L. Zeng, J. Zhang, K. Hu, et al., Microbial characteristics and genomic analysis of an ST11 carbapenem-resistant Klebsiella pneumoniae strain carrying blaKPC-2 conjugative drug-resistant plasmid, Front. Public Health 9 (2022) 809753.
[8] L. Assoni, R. Girardello, T.R. Converso, M. Darrieux, Current stage in the development of Klebsiella pneumoniae vaccines, Infect. Dis. Ther. 10 (4) (2021) 2157–2175.
[9] J. Dey, S.R. Mahapatra, S. Lata, S. Patro, N. Misra, M. Suar, Exploring Klebsiella pneumoniae capsule polysaccharide proteins to design multiepitope subunit vaccine to fight against pneumonia, Expert Rev. Vaccines 21 (4) (2022) 569–587.
[10] S.R. Mahapatra, J. Dey, T. Kaur, et al., Immunoinformatics and molecular docking studies reveal a novel Multi-Epitope peptide vaccine against pneumonia infection, Vaccine 39 (42) (2021) 6221–6237.
[11] S.A. Sami, K.K.S. Marma, S. Mahmud, et al., Designing of a multi-epitope vaccine against the structural proteins of Marburg virus exploiting the immunoinformatics approach, ACS Omega 6 (47) (2021) 32043–32071.
[12] M. Yu, Y. Zhu, Y. Li, et al., Design of a novel multi-epitope vaccine against Echinococcus granulosus in immunoinformatics, Front. Immunol. 1 2 (2021) 668492.
[13] J. Dey, S.R. Mahapatra, P. Singh, et al., B and T cell epitope-based peptides predicted from clumping factor protein of Staphylococcus aureus as vaccine targets, Microb. Pathog. 160 (2021) 105171.
[14] S. Sahoo, S.R. Mahapatra, B.K. Parida, et al., DBCOVP: a database of coronavirus virulent glycoproteins, Comput. Biol. Med. 129 (2021) 104131.
[15] S.R. Mahapatra, J. Dey, G.S. Kushwaha, et al., Immunoinformatic approach employing modeling and simulation to design a novel vaccine construct targeting MDR efflux pumps to confer wide protection against typhoidal Salmonella serovars, J. Biomol. Struct. Dyn. 40 (22) (2022) 11809–11821.
[16] L.P.P. Patro, T. Rathinavelan, Targeting the sugary Armor of Klebsiella species, Front. Cell. Infect. Microbiol. 9 (2019) 367.
[17] L. Babu, S.R. Uppalapati, M.H. Sripathy, P.N. Reddy, Evaluation of recombinant multi-epitope outer membrane protein-based Klebsiella pneumoniae subunit vaccine in Mouse model, Front. Microbiol. 8 (2017) 1805.
[18] M.M. Cameranesi, J. Paganini, A.S. Limansky, et al., Acquisition of plasmids conferring carbapenem and aminoglycoside resistance and loss of surface-exposed macromolecule structures as strategies for the adaptation of Acinetobacter baumannii CC104O/CC15P strains to the clinical setting, Microb. Genom. 6 (9) (2020) mgen000360.

[19] R. Cai, M. Wu, H. Zhang, et al., A Smooth-type, Phage-resistant Klebsiella pneumoniae mutant strain Reveals that OmpC is indispensable for infection by phage GH-K3, Appl. Environ. Microbiol. 84 (21) (2018) e01585-18.
[20] N. Iwanaga, K. Chen, H. Yang, et al., Vaccine-driven lung TRM cells provide immunity against Klebsiella via fibroblast IL-17R signaling, Sci Immunol 6 (63) (2021) eabf1198.
[21] P. Kurupati, B.K. Teh, G. Kumarasinghe, C.L. Poh, Identification of vaccine candidate antigens of an ESBL producing Klebsiella pneumoniae clinical strain by immunoproteome analysis, Proteomics 6 (3) (2006) 836–844.
[22] A. Rocker, J.A. Lacey, M.J. Belousoff, et al., Global trends in Proteome Remodeling of the outer membrane modulate antimicrobial Permeability in Klebsiella pneumoniae, mBio 11 (2) (2020) e00603–e00620.
[23] K. Zhang, X. Wu, Y. Shi, X. Gou, J. Huang, Immunogenicity of H5N1 influenza vaccines in elderly adults: a systematic review and meta-analysis, Hum. Vaccines Immunother. 17 (2) (2021) 475–484.
[24] R. Chatterjee, P. Sahoo, S.R. Mahapatra, et al., Development of a conserved chimeric vaccine for Induction of strong immune response against Staphylococcus aureus using immunoinformatics approaches, Vaccines 9 (9) (2021) 1038.
[25] M.R. Wilkins, E. Gasteiger, A. Bairoch, et al., Protein identification and analysis tools in the ExPASy server, Methods Mol. Biol. 112 (1999) 531–552.
[26] G. Obando-Pereda, Can molecular mimicry explain the cytokine storm of SARS-CoV-2?: an in silico approach, J. Med. Virol. 93 (9) (2021) 5350–5357.
[27] R. Lavigne, D. Seto, P. Mahadevan, H.W. Ackermann, A.M. Kropinski, Unifying classical and molecular taxonomic classification: analysis of the Podoviridae using BLASTP-based tools, Res. Microbiol. 159 (5) (2008) 406–414.
[28] B.P. Alcock, A.R. Raphenya, T.T.Y. Lau, et al., Card 2020: antibiotic resistome surveillance with the comprehensive antibiotic resistance database, Nucleic Acids Res. 48 (D1) (2020) D517–D525.
[29] A.M. Waterhouse, J.B. Procter, D.M. Martin, M. Clamp, G.J. Barton, Jalview Version 2–a multiple sequence alignment editor and analysis workbench, Bioinformatics 25 (9) (2009) 1189–1191.
[30] E.M. Holgersen, S. Gandhi, Y. Zhou, et al., Transcriptome-wide Off-target effects of Steric-Blocking Oligonucleotides, Nucleic Acid Therapeut. 31 (6) (2021) 392–403.
[31] F. Teufel, J.J. Almagro Armenteros, A.R. Johansen, et al., SignalP 6.0 predicts all five types of signal peptides using protein language models [published online ahead of print, 2022 Jan 3], Nat. Biotechnol. (2022), https://doi.org/10.1038/s41587-021-01156-3.
[32] V. Solanki, M. Tiwari, V. Tiwari, Prioritization of potential vaccine targets using comparative proteomics and designing of the chimeric multi-epitope vaccine against Pseudomonas aeruginosa, Sci. Rep. 9 (1) (2019) 5240.
[33] S. Saha, G.P. Raghava, Prediction of continuous B-cell epitopes in an antigen using recurrent neural network, Proteins 65 (1) (2006) 40–48.
[34] J. Jumper, R. Evans, A. Pritzel, et al., Highly accurate protein structure prediction with AlphaFold, Nature 596 (7873) (2021) 583–589.
[35] J. Ponomarenko, H.H. Bui, W. Li, et al., ElliPro: a new structure-based tool for the prediction of antibody epitopes, BMC Bioinf. 9 (2008) 514.
[36] M. Shams, H. Nourmohammadi, H. Majidiani, et al., Engineering a multi-epitope vaccine candidate against Leishmania infantum using comprehensive Immunoinformatics methods, Biologia 77 (1) (2022) 277–289.
[37] E.F. Alfano, E.M. Lentz, D. Bellido, et al., Expression of the Multimeric and highly immunogenic Brucella spp. Lumazine Synthase fused to Bovine Rotavirus VP8d as a Scaffold for antigen production in Tobacco Chloroplasts, Front. Plant Sci. 6 (2015) 1170.
[38] J. Dey, S.R. Mahapatra, S. Patnaik, et al., Molecular Characterization and designing of a novel multiepitope vaccine construct against Pseudomonas aeruginosa, Int. J. Pept. Res. Therapeut. 28 (2) (2022) 49.
[39] H.H. Bui, J. Sidney, K. Dinh, S. Southwood, M.J. Newman, A. Sette, Predicting population coverage of T-cell epitope-based diagnostics and vaccines, BMC Bioinf. 7 (2006) 153.
[40] C.N. Magnan, A. Randall, P. Baldi, SOLpro: accurate sequence-based prediction of protein solubility, Bioinformatics 25 (17) (2009) 2200–2207.
[41] C. Geourjon, G. Deléage, SOPMA: significant improvements in protein secondary structure prediction by consensus prediction from multiple alignments, Comput. Appl. Biosci. 11 (6) (1995) 681–684.
[42] J. Ko, H. Park, L. Heo, C. Seok, GalaxyWEB server for protein structure prediction and refinement, Nucleic Acids Res. 40 (2012) W294–W297. Web Server issue).
[43] M. Wiederstein, M.J. Sippl, ProSA-web: interactive web service for the recognition of errors in three-dimensional structures of proteins, Nucleic Acids Res. 35 (2007) W407–W410. Web Server issue).
[44] D.B. Craig, A.A. Dombkowski, Disulfide by Design 2.0: a web-based tool for disulfide engineering in proteins, BMC Bioinf. 14 (2013) 346.
[45] S. Aslam, U.A. Ashfaq, T. Zia, et al., Proteome based mapping and reverse vaccinology techniques to contrive multi-epitope based subunit vaccine (MEBSV) against Streptococcus pyogenes, Infect. Genet. Evol. 100 (2022) 105259.
[46] X. Zhang, K. Li, S. Zhong, et al., Immunotherapeutic value of MAP1LC3C and its candidate FDA-Approved drugs identified by Pan-Cancer analysis, Virtual screening and Sensitivity analysis, Front. Pharmacol. 13 (2022) 863856.
[47] J.R. López-Blanco, J.I. Aliaga, E.S. Quintana-Ortí, P. Chacón, iMODS: internal coordinates normal mode analysis server, Nucleic Acids Res. 42 (2014) W271–W276. Web Server issue).
[48] M.S. Robescu, G. Loprete, M. Gasparotto, et al., The family Keeps on growing: Four novel Fungal OYEs Characterized, Int. J. Mol. Sci. 23 (6) (2022) 3050.
[49] C.D. Wassman, R. Baronio, Ö. Demir, et al., Computational identification of a transiently open L1/S3 pocket for reactivation of mutant p53, Nat. Commun. 4 (2013) 1407.
[50] J.A. Maier, C. Martinez, K. Kasavajhala, L. Wickstrom, K.E. Hauser, C. Simmerling, ff14SB: improving the accuracy of protein side chain and backbone parameters from ff99SB, J. Chem. Theor. Comput. 11 (8) (2015) 3696–3713.
[51] H. Okumura, S.G. Itoh, Molecular dynamics simulation studies on the Aggregation of Amyloid-β peptides and their Disaggregation by Ultrasonic wave and Infrared laser Irradiation, Molecules 27 (8) (2022) 2483.
[52] R.N. Shinde, S. Karthikeyan, B. Singh, Molecular dynamics studies unravel role of conserved residues responsible for movement of ions into active site of DHBPS, Sci. Rep. 7 (2017) 40452.
[53] A.O. Elzupir, Caffeine and caffeine-containing pharmaceuticals as promising inhibitors for 3-chymotrypsin-like protease of SARS-CoV-2, J. Biomol. Struct. Dyn. 40 (5) (2022) 2113–2120.
[54] G. Bhattacharje, A. Ghosh, A.K. Das, Understanding the Mannose Transfer mechanism of Mycobacterial Phosphatidyl-myo-inositol Mannosyltransferase A from molecular dynamics simulations, ACS Omega 7 (23) (2022) 19288–19304.
[55] N. Rapin, O. Lund, M. Bernaschi, F. Castiglione, Computational immunology meets bioinformatics: the use of prediction tools for molecular binding in the simulation of the immune system, PLoS One 5 (4) (2010) e9862.
[56] A.R. Gruber, R. Lorenz, S.H. Bernhart, R. Neuböck, I.L. Hofacker, The Vienna RNA websuite, Nucleic Acids Res. 36 (2008) W70–W74. Web Server issue).
[57] J. Perdigão, A. Modesto, A.L. Pereira, et al., Whole-genome sequencing resolves a polyclonal outbreak by extended-spectrum beta-lactam and carbapenem-resistant Klebsiella pneumoniae in a Portuguese tertiary-care hospital, Microb. Genom. 7 (6) (2019) 000349.
[58] J. Findlay, L. Poirel, M. Juhas, P. Nordmann, KPC-mediated resistance to ceftazidime-avibactam and Collateral effects in Klebsiella pneumoniae, Antimicrob. Agents Chemother. 65 (9) (2021) e0089021.
[59] S. Gul, S. Ahmad, A. Ullah, et al., Designing a recombinant vaccine against Providencia rettgeri using immunoinformatics approach, Vaccines 10 (2) (2022) 189.
[60] D. Cai, H. Wang, P. He, et al., A novel strategy to improve protein secretion via overexpression of the SppA signal peptide peptidase in Bacillus licheniformis, Microb. Cell Factories 16 (1) (2017) 70.
[61] S.R. Mahapatra, S. Sahoo, B. Dehury, et al., Designing an efficient multi-epitope vaccine displaying interactions with diverse HLA molecules for an efficient humoral and cellular immune response to prevent COVID-19 infection, Expert Rev. Vaccines 19 (9) (2020) 871–885.
[62] M. Alizadeh, H. Amini-Khoei, S. Tahmasebian, et al., Designing a novel multi-epitope vaccine against Ebola virus using reverse vaccinology approach, Sci. Rep. 12 (1) (2022) 7757.
[63] C. Aguilar-Bonavides, R. Sanchez-Arias, C. Lanzas, Accurate prediction of major histocompatibility complex class II epitopes by sparse representation via ℓ1-minimization, BioData Min. 7 (2014) 23.

[64] K. Rawal, R. Sinha, B.A. Abbasi, et al., Identification of vaccine targets in pathogens and design of a vaccine using computational approaches, Sci. Rep. 11 (1) (2021) 17626.
[65] A. Ouattara, A. Dwivedi, M. Adams, et al., An in silico analysis of Malaria pre-Erythrocytic-stage antigens Interpreting worldwide Genetic data to suggest vaccine candidate Variants and epitopes, Microorganisms 10 (6) (2022) 1090.
[66] E. Jahangirian, G.A. Jamal, M. Nouroozi, A. Mohammadpour, A reverse vaccinology and immunoinformatics approach for designing a multiepitope vaccine against SARS-CoV-2, Immunogenetics 73 (6) (2021) 459–477.
[67] M. Sana, A. Javed, S. Babar Jamal, M. Junaid, M. Faheem, Development of multivalent vaccine targeting M segment of Crimean Congo Hemorrhagic Fever Virus (CCHFV) using immunoinformatic approaches, Saudi J. Biol. Sci. 29 (4) (2022) 2372–2388.
[68] A. Maleki, G. Russo, G.A. Parasiliti Palumbo, F. Pappalardo, In silico design of recombinant multi-epitope vaccine against influenza A virus, BMC Bioinf. 22 (Suppl 14) (2022) 617.
[69] S.I. Islam, M.J. Mou, S. Sanjida, Application of reverse vaccinology to design a multi-epitope subunit vaccine against a new strain of Aeromonas veronii, J. Genet. Eng. Biotechnol. 20 (1) (2022) 118.
[70] H. Tarrahimofrad, S. Rahimnahal, J. Zamani, E. Jahangirian, S. Aminzadeh, Designing a multi-epitope vaccine to provoke the robust immune response against influenza A H7N9, Sci. Rep. 11 (1) (2021) 24485.
[71] J.M. Royal, N. Matoba, Therapeutic potential of cholera toxin B subunit for the treatment of Inflammatory diseases of the Mucosa, Toxins 9 (12) (2017) 379.
[72] S.A. Sami, K.K.S. Marma, S. Mahmud, et al., Designing of a multi-epitope vaccine against the structural proteins of Marburg virus exploiting the immunoinformatics approach, ACS Omega 6 (47) (2021) 32043–32071.
[73] Y. Li, X. Liu, Y. Zhu, et al., Bioinformatic prediction of epitopes in the Emy162 antigen of Echinococcus multilocularis, Exp. Ther. Med. 6 (2) (2013) 335–340.
[74] A.K. Meyers, X. Zhu, The NLRP3 Inflammasome: Metabolic Regulation and contribution to Inflammaging, Cells 9 (8) (2020) 1808.
[75] J.A. Kovacs, P. Chacón, R. Abagyan, Predictions of protein flexibility: first-order measures, Proteins 56 (4) (2004) 661–668.
[76] T. Ichiye, M. Karplus, Collective motions in proteins: a covariance analysis of atomic fluctuations in molecular dynamics and normal mode simulations, Proteins 11 (3) (1991) 205–217.
[77] S.R. Khan, A.C. van der Burgh, R.P. Peeters, P.M. van Hagen, V.A.S.H. Dalm, L. Chaker, Determinants of Serum Immunoglobulin levels: a systematic review and meta-analysis, Front. Immunol. 12 (2021) 664526.
[78] A. Sethi, N. Kulkarni, S. Sonar, G. Lal, Role of miRNAs in CD4 T cell plasticity during inflammation and tolerance, Front. Genet. 4 (2013) 8.
[79] H. Al Tbeishat, Novel in Silico mRNA vaccine design exploiting proteins of M. tuberculosis that modulates host immune responses by inducing epigenetic modifications, Sci. Rep. 12 (1) (2022) 4645.
[80] M.M. Rahman, J.A. Puspo, A.A. Adib, et al., An immunoinformatics prediction of novel multi-epitope vaccines candidate against surface antigens of Nipah virus, Int. J. Pept. Res. Therapeut. 28 (4) (2022) 123.